

Kaonic modes in hyperonic matter and *p*-wave kaon condensation

Takumi Muto*

*Department of Physics, Chiba Institute of Technology,
2-1-1 Shibazono, Narashino, Chiba 275-0023, Japan*

(May 20, 2019)

Abstract

Kaon excitations (kaonic modes) are investigated in hyperonic matter, where hyperons (Λ , Σ^- , Ξ^-) are mixed in the ground state of neutron-star matter. *P*-wave kaon-baryon interactions as well as the *s*-wave interactions are taken into account within chiral effective Lagrangian, and the nonrelativistic effective baryon-baryon interactions are incorporated. When the hyperon Λ is more abundant than the proton at high baryon density, a proton-particle- Λ -hole mode, which has the K^+ quantum number, appears in addition to other particle-hole modes with the K^- quantum number. It is shown that the system becomes unstable with respect to a spontaneous creation of a pair of the particle-hole modes with K^+ and K^- quantum numbers, stemming from the *p*-wave kaon-baryon interaction. The onset density of this *p*-wave kaon condensation may be lower than that of the *s*-wave K^- condensation.

PACS: 05.30.Jp, 11.55.Fv, 13.75.Jz, 26.60.+c

Keywords: kaon-baryon interaction, neutron stars, dispersion relations, kaon condensation

*Email address; muto@pf.it-chiba.ac.jp

I. INTRODUCTION

Kaon condensation in high density matter has been investigated extensively from various points of view [1–6]. Its existence makes the equation of state (EOS) of high density matter much softened, which affects static properties of neutron stars [4,7–9] and also dynamical evolution of protoneutron stars [10,11]. A kaon condensate also leads to rapid cooling of neutron stars via enhanced neutrino emissions [7,12–15].

The driving force for kaon condensation is the *s*-wave kaon-nucleon (KN) interaction which consists of the scalar attraction simulated by the KN sigma term Σ_{KN} and the vector interaction corresponding to the Tomozawa Weinberg term. In neutron-star matter, the lowest excitation energy ω_{\min} of the antikaon decreases with baryon number density ρ_B due to the *s*-wave KN attraction. At a critical density, ω_{\min} becomes equal to the kaon chemical potential μ_K , and the K^- appears macroscopically as a Bose-Einstein condensate (BEC).¹ The critical density ρ_B^C has been estimated as $\rho_B^C = 3 - 4\rho_0$ with ρ_0 ($= 0.16 \text{ fm}^{-3}$) being the nuclear saturation density [1–6]. Recently, some authors examined the possibility of kaon condensation in neutron stars by taking into account many-body effects such as the Pauli-blocking and the nucleon-nucleon correlations [16,17].

Studies of kaon condensation stimulated theoretical investigations of in-medium kaon properties with reference to the kaon-nucleon scattering [18–21], kaonic atoms [22–25], and heavy-ion collisions [26–30]. The momentum dependence of kaon optical potentials in a nuclear medium has also been discussed, which may serve as unified understanding of these phenomena [31–33]. Although there is still a debate concerning the strength of the kaon optical potential, recent experimental results on the subthreshold K^+K^- production in relativistic heavy-ion collisions and proton-nucleus collisions suggest a substantial decrease in the antikaon effective mass [34–36]. Based on the strongly attractive kaonic potential, a possibility of kaonic nuclei has been proposed [37,38].

So far, kaon condensation has been considered mostly in neutron-star matter consisting of neutrons, protons and leptons in chemical equilibrium. However, hyperons (Λ , Ξ^- , $\Sigma^- \dots$) may appear in neutron-star matter. The possible existence of hyperonic matter, where hyperons are mixed as well as neutrons, protons, and leptons in the ground state of neutron-star matter, has been suggested by several authors [39–53].

Recent development of hypernuclear experiments enables us to discuss the hyperon-mixing problem in highly dense matter in a realistic situation. It has been shown that hyperons appear at a baryon number density $\rho_B = 2 \sim 3\rho_0$ based on the relativistic mean-field (RMF) models [42–45], relativistic Hartree-Fock methods [46], the nonrelativistic reaction matrix theory [47,48], the nonrelativistic effective baryon-baryon potential models [49–51], etc. [52,53] The hyperonic matter is also relevant to static and dynamic properties of neutron stars [54,55] and thermal evolution of neutron stars via rapid cooling [56].

The existence region of kaon condensation and hyperons may overlap each other, so that the competition or coexistence problem of these phases has to be clarified. Concerning this problem, it has been pointed out that a critical density of K^- condensation, which may be realized from hyperonic matter, is pushed up to a higher baryon number density

¹The kaon chemical potential μ_K is equal to the electron chemical potential μ_e in chemical equilibrium. We put $\mu_K = \mu_e = \mu$, and call μ the charge chemical potential throughout this paper.

in the presence of the negatively charged hyperons in comparison with the neutron-star matter consisting of only neutrons, protons, and leptons [43,44]: The negative charge of the system is carried by the negatively charged hyperons in place of the electrons as the hyperon-mixing develops, making up with the positive charge and satisfying the charge neutrality. Accordingly, the number of the electrons n_e and the charge chemical potential μ [$=(3\pi^2 n_e)^{1/3}$] get smaller with the increase in the baryon number density, which makes the onset condition for kaon condensation, $\omega_{\min} = \mu$, difficult to satisfy². In Refs. [43,44], only the *s*-wave kaon-baryon interaction has been taken into account. However, there is the *p*-wave kaon-baryon interaction with Yukawa couplings, which may affect kaon dynamics in dense matter crucially as well as the *s*-wave interaction. In this context, interrelation between kaons and hyperons has been discussed through the introduction of a “kaesobar” which is a linear combination of the K^- and Σ^- -particle-neutron-hole states produced by the *p*-wave interaction [26,57]. On the other hand, the effects of the *p*-wave kaon-baryon interaction on kaon condensation have been considered in neutron-star matter where hyperons are not mixed in the ground state of dense matter [58,59]. In Ref. [58], the kaon-baryon interaction has been taken into account within chiral effective Lagrangian. It has been shown that the *s*-wave K^- condensation sets in at a lower density, and at a higher density, the *p*-wave K^- condensation is realized accompanying hyperon excitation in the form of quasi-particles which are superimposed states of nucleons and hyperons. The K^- mode has been shown to be relevant to the onset of *p*-wave K^- condensation.³ In Ref. [59], pionic intermediate states, kaon fluctuations and residual interaction have been incorporated in addition to the *s*-wave and *p*-wave kaon-baryon interactions. It has been shown that the energy of a low-lying Λ -particle-proton-hole branch becomes negative beyond some density, leading to a first-order phase transition to proton matter accompanying kaon condensation.

In this paper, we consider kaon dynamics and mechanisms of kaon condensation in *hyperonic matter* by taking into account the *p*-wave kaon-baryon interaction. We discuss in-medium properties of kaons by obtaining the kaon dispersion relations in hyperonic matter. Kaon-baryon interactions for both the *s*-wave and *p*-wave type are incorporated within the effective chiral Lagrangian, while other baryon-baryon interactions are supplemented by the use of the nonrelativistic effective interactions. We show that a low-lying proton-particle- Λ -hole mode with the K^+ quantum number develops at high densities. This mode, together with the other particle-hole modes carrying the K^- quantum number, leads to a new mechanism of kaon condensation stemming from the *p*-wave kaon-baryon interaction.⁴

The paper is organized as follows. Section II gives the formulation to obtain the kaonic modes in hyperonic matter. In Sec. III, numerical results are given. Summary and concluding remarks are devoted in Sec. IV. In the Appendix, the expression for the potential energy density which is used in the formulation is presented.

²The same situation is applied for the neutral hyperons, e.g., Λ : As the Λ appears, the electron is absorbed by the process, $p + e^- \rightarrow \Lambda + \nu_e$ (see III B).

³Throughout this paper, the K^- and K^+ denote the kaonic modes which reduce to free kaons in vacuum ($\rho_B \rightarrow 0$), and are distinguished from other particle-hole modes carrying the K^\pm quantum numbers.

⁴ Part of this work has been briefly reported in Ref. [60].

II. FORMULATION

A. Kaon-baryon interaction

We start with the effective chiral $SU(3)_L \times SU(3)_R$ Lagrangian used by Kaplan and Nelson [1] for the kaon-baryon interaction.⁵

$$\begin{aligned} \mathcal{L} = & \frac{1}{4}f^2 \text{Tr} \partial^\mu \Sigma^\dagger \partial_\mu \Sigma + \frac{1}{2}f^2 \Lambda_{\chi\text{SB}} (\text{Tr} M(\Sigma - 1) + \text{h.c.}) \\ & + \text{Tr} \overline{\Psi} (i\partial - M_B) \Psi + \text{Tr} \overline{\Psi} i \gamma^\mu [V_\mu, \Psi] + D \text{Tr} \overline{\Psi} \gamma^\mu \gamma^5 \{A_\mu, \Psi\} + F \text{Tr} \overline{\Psi} \gamma^\mu \gamma^5 [A_\mu, \Psi] \\ & + a_1 \text{Tr} \overline{\Psi} (\xi M^\dagger \xi + \text{h.c.}) \Psi + a_2 \text{Tr} \overline{\Psi} \Psi (\xi M^\dagger \xi + \text{h.c.}) + a_3 (\text{Tr} M \Sigma + \text{h.c.}) \text{Tr} \overline{\Psi} \Psi, \end{aligned} \quad (1)$$

where f ($\sim f_\pi = 93$ MeV) is the meson decay constant, Σ is the nonlinear meson field, $\Sigma \equiv e^{2i\Pi/f}$, in terms of the octet meson Π , which is represented as

$$\Pi = \pi_a T_a = \frac{1}{\sqrt{2}} \begin{pmatrix} \pi^0/\sqrt{2} + \eta/\sqrt{6} & \pi^+ & K^+ \\ \pi^- & -\pi^0/\sqrt{2} + \eta/\sqrt{6} & K^0 \\ K^- & \overline{K}^0 & -\sqrt{\frac{2}{3}}\eta \end{pmatrix} \quad (2)$$

with the Nambu-Goldstone bosons π_a and the $SU(3)$ generators T_a ($a = 1 \sim 8$). $\Lambda_{\chi\text{SB}}$ is the chiral symmetry breaking scale, ~ 1 GeV, M the mass matrix which is defined as $M \equiv \text{diag}(m_u, m_d, m_s)$ with the quark masses m_i , and M_B is the baryon mass generated as a consequence of spontaneous chiral symmetry breakdown. The baryon fields are given as the spin 1/2 octet Ψ ,

$$\Psi = \begin{pmatrix} \Sigma^0/\sqrt{2} + \Lambda/\sqrt{6} & \Sigma^+ & p \\ \Sigma^- & -\Sigma^0/\sqrt{2} + \Lambda/\sqrt{6} & n \\ \Xi^- & \Xi^0 & -2\Lambda/\sqrt{6} \end{pmatrix}. \quad (3)$$

Baryons couple with mesons through the mesonic vector current V_μ , which is defined by $V_\mu \equiv 1/2(\xi^\dagger \partial_\mu \xi + \xi \partial_\mu \xi^\dagger)$ with $\xi \equiv \Sigma^{1/2}$, and the axial vector current A_μ , defined by $A_\mu \equiv i/2(\xi^\dagger \partial_\mu \xi - \xi \partial_\mu \xi^\dagger)$. In the nonrelativistic limit, the fourth term including V_μ in Eq. (1) reduces to the s -wave vector interaction, and the fifth and sixth terms to the p -wave interaction. The last three terms in Eq. (1) represent the s -wave meson-baryon scalar interaction, which explicitly breaks down chiral symmetry.

Throughout this paper, we take the same set of parameters as those in Ref. [1]: The axial vector coupling constants D and F are determined from the weak decays of the baryon octet states and are chosen as $D=0.81$ and $F=0.44$. The quark masses are taken to be $m_u=6$ MeV, $m_d=12$ MeV and $m_s=240$ MeV. With these values for m_i , the parameters a_1 and a_2 are fixed so as to give the empirical octet baryon mass splittings and given as $a_1=-0.28$, $a_2=0.56$.

The parameter a_3 is related to the “ πN and KN sigma terms” which simulate the s -wave meson-baryon scalar interactions through the relations, $\Sigma_{\pi N} = -(a_1+2a_3)(m_u+m_d)$, $\Sigma_{Kp} = -(a_1+a_2+2a_3)(m_u+m_s)$, and $\Sigma_{Kn} = -(a_2+2a_3)(m_u+m_s)$. Considering that there is some ambiguity about these values, we take a_3 to be $a_3 = -0.9$ and -1.1 , which

⁵ We use the units in which $\hbar=c=k_B=1$ throughout this paper.

yields $\Sigma_{\pi N}=37$ MeV, $\Sigma_{Kp}=374$ MeV, $\Sigma_{Kn}=305$ MeV for $a_3 = -0.9$, and $\Sigma_{\pi N}=45$ MeV, $\Sigma_{Kp}=472$ MeV, $\Sigma_{Kn}=403$ MeV for $a_3 = -1.1$.

In this paper, we mainly concentrate on the kaon dispersion relations in hyperonic matter and onset mechanisms of kaon condensation. Expecting that we can also discuss the EOS of a fully-developed kaon-condensed phase beyond the onset density [65] within the same framework, we give here a formulation to elucidate both issues in a unified way: First, the energy density of the kaon-condensed phase, \mathcal{E}_{eff} , is obtained, and second, the kaon inverse propagator $D_K^{-1}(\omega, \mathbf{k}; \rho_B)$ is obtained from the expansion of the energy density expression with respect to the classical kaon field K^{cl} as $\mathcal{E}_{\text{eff}}(|K^{\text{cl}}|) = \mathcal{E}_{\text{eff}}(|K^{\text{cl}}| = 0) - D_K^{-1}(\omega = \mu, \mathbf{k}; \rho_B)|K^{\text{cl}}|^2 + O(|K^{\text{cl}}|^4)$.⁶

The kaon inverse propagator D_K^{-1} includes the self energy which is related to the forward KN scattering amplitudes. It is to be noted that there are different ways of off-shell extrapolation from the KN scattering amplitudes in obtaining the kaon self energy: One is derived from chiral perturbation theory and the other is based on low energy theorems of current algebra and PCAC (partially conservation of axial-vector current). These approaches lead to different off-shell properties of the kaon excitation energy [61,62,2,4]. The relations between these approaches have been discussed [63,64]. Based on the former way with the chiral effective Lagrangian Eq. (1), the s -wave KN scattering amplitudes near threshold cannot be reproduced empirically without higher order terms in chiral expansion and a pole contribution from the $\Lambda(1405)$ [62,2,19]. These corrections enter into the kaon self energy. Nevertheless, It has been shown that part of the higher order terms for K^- , the range term [$\propto \omega(K^-)^2$], becomes small in high-density matter, since the K^- excitation energy $\omega(K^-)$ decreases with density owing to the s -wave KN attractive interaction. Furthermore, the pole contribution from the $\Lambda(1405)$ becomes negligible since the K^-N threshold lies far below the pole of the $\Lambda(1405)$ at high density due to the decrease in $\omega(K^-)$. Hence these corrections become irrelevant to the s -wave K^- excitation energy in high-density matter [2,4,19,62], while the K^+ excitation energy is largely changed due to the repulsive effects from the higher-order corrections. When hyperons are incorporated, extra terms next to leading order, coming from the p -wave kaon-baryon interaction, contribute to the self energy. These terms are typically proportional to $(k^\mu)^2 = \omega^2 - \mathbf{k}^2$, and are responsible for reproducing the low-energy data on pion- and photon-induced kaon production and elastic and inelastic K^-p scatterings [66,67]. In hyperonic matter, several kaonic modes of particle-hole excitations appear in addition to the K^\pm due to the p -wave interaction, as shown in Sec. III, and the excitation energies for these modes are small, being of order of the s -wave K^- energy. Thus we expect that the higher order terms coming from the p -wave interaction have minor effects on the kaonic modes as far as the kaon momentum is not very large, i.e., $|\mathbf{k}| = O(\omega)$ except for the K^+ . Hence, throughout this paper, we are based on the chiral effective Lagrangian Eq. (1), and don't take into account higher order terms in chiral expansion with respect to $M/\Lambda_{\chi SB}$ and $\partial/\Lambda_{\chi SB}$. Quantitative evaluation including these higher order terms remains to be a future investigation.

⁶ Similar methods have been utilized in Refs. [4,58].

B. Effective energy density

For simplicity, we take only the Λ , Σ^- , and Ξ^- for hyperons in addition to the proton (p), neutron (n) for nucleons and the ultrarelativistic electron for leptons. The other hyperons, Σ^0 , Σ^+ and Ξ^0 , are supposed to be irrelevant because they appear in higher densities due to their heavy baryon masses and due to the fact that the electron chemical potential does not assist to satisfy the threshold condition in contrast to the case of the negatively charged hyperons.

We consider charged kaon condensation in chemically-equilibrated hyperonic matter, and neglect other mesons in the octet meson field Σ . The classical kaon field is then assumed to be a plane wave type:

$$K^{\pm, \text{cl}}(\mathbf{r}, t) = \frac{f}{\sqrt{2}} \theta e^{\pm i(\mu_K t - \mathbf{k} \cdot \mathbf{r})}, \quad (4)$$

where θ is a chiral angle which means an amplitude of a condensate, μ_K the kaon chemical potential, and \mathbf{k} is the kaon momentum.

The effective Hamiltonian \mathcal{H}_{eff} is derived with the introduction of the charge chemical potential $\mu (= \mu_K = \mu_e)$ by a charge neutrality condition, and is separated into baryon, meson and lepton parts:

$$\mathcal{H}_{\text{eff}} = \mathcal{H}_{\text{eff}}^B + \mathcal{H}_{\text{eff}}^M + \mathcal{H}_{\text{eff}}^e, \quad (5)$$

where $\mathcal{H}_{\text{eff}}^B = \mathcal{H}^B + \mu \rho_Q^B$, $\mathcal{H}_{\text{eff}}^M = \mathcal{H}^M + \mu \rho_Q^M$, and $\mathcal{H}_{\text{eff}}^e = \mathcal{H}^e + \mu \rho_Q^e$ with the charge density operators ρ_Q^i ($i = B, M, e$).

The axial vector coupling terms in the baryonic part $\mathcal{H}_{\text{eff}}^B$ have space-time dependent factors $\exp(\pm i p_K \cdot x)$ with a four momentum $p_K^\mu [= (\mu_K, \mathbf{k})]$. These factors are eliminated by transformation of the baryon bases $\psi^T = (p, \Lambda, \Xi^-, n, \Sigma^-)$ as $\psi^T \rightarrow \tilde{\psi}^T = (e^{-i p_K \cdot x} p, \Lambda, e^{i p_K \cdot x} \Xi^-, e^{-i p_K \cdot x/2} n, e^{i p_K \cdot x/2} \Sigma^-)$. By this transformation, the momentum of each baryon is shifted by $\mathcal{V}_3 \mathbf{k}$, where \mathcal{V}_3 is the V -spin defined by $\mathcal{V}_3 = \frac{1}{2} (I_3 + \frac{3}{2} Y)$ with the third component of the isospin I_3 and the hypercharge Y . After making the Foldy-Wouthuysen-Tani transformation for $\mathcal{H}_{\text{eff}}^B$ and expanding it up to $O(1/M_N)$ with M_N the nucleon mass, one obtains the baryonic part of the Hamiltonian in a nonrelativistic form as $\tilde{\mathcal{H}}_{\text{eff}}^B = \tilde{\psi}^\dagger H_{\text{eff}}^B \tilde{\psi}$ with

$$H_{\text{eff}}^B = \begin{pmatrix} H_{pp} & H_{p\Lambda} & H_{p\Xi^-} & 0 & 0 \\ H_{\Lambda p} & H_{\Lambda\Lambda} & H_{\Lambda\Xi^-} & 0 & 0 \\ H_{\Xi^- p} & H_{\Xi^-\Lambda} & H_{\Xi^-\Xi^-} & 0 & 0 \\ 0 & 0 & 0 & H_{nn} & H_{n\Sigma^-} \\ 0 & 0 & 0 & H_{\Sigma^- n} & H_{\Sigma^-\Sigma^-} \end{pmatrix}, \quad (6)$$

where the nonvanishing matrix elements are given by

$$H_{pp} = \frac{1}{2M_N} \left\{ (\mathbf{p} - \mathbf{k} \cos \theta)^2 + \left(\frac{1}{2} g_{\Lambda p} \mu \sin \theta \right)^2 \right\} + \mu \cos \theta - \Sigma_{Kp} (1 - \cos \theta)$$

$$H_{p\Lambda} = \frac{i}{2} g_{\Lambda p} \sin \theta \left\{ \mathbf{k} - \frac{\mu}{2M_N} (2\mathbf{p} - \mathbf{k} \cos \theta) \right\} \cdot \boldsymbol{\sigma} = H_{\Lambda p}^*$$

$$H_{p\Xi^-} = \frac{1}{8M_N} g_{\Lambda p} g_{\Xi^-\Lambda} (\mu \sin \theta)^2 = H_{\Xi^- p}$$

$$\begin{aligned}
H_{\Lambda\Lambda} &= \frac{1}{2M_N} \left[\mathbf{p}^2 + \left\{ \left(\frac{g_{\Lambda p}}{2} \right)^2 + \left(\frac{g_{\Xi^-\Lambda}}{2} \right)^2 \right\} (\mu \sin \theta)^2 \right] + \delta M_{\Lambda N} - \Sigma_{K\Lambda} (1 - \cos \theta) \\
H_{\Lambda\Xi^-} &= -\frac{i}{2} g_{\Xi^-\Lambda} \sin \theta \left\{ \mathbf{k} - \frac{\mu}{2M_N} (2\mathbf{p} + \mathbf{k} \cos \theta) \right\} \cdot \boldsymbol{\sigma} = H_{\Xi^-\Lambda}^* \\
H_{\Xi^-\Xi^-} &= \frac{1}{2M_N} \left\{ (\mathbf{p} + \mathbf{k} \cos \theta)^2 + \left(\frac{1}{2} g_{\Xi^-\Lambda} \mu \sin \theta \right)^2 \right\} + \delta M_{\Xi^-N} - \mu \cos \theta - \Sigma_{K\Xi^-} (1 - \cos \theta) \\
H_{nn} &= \frac{1}{2M_N} \left\{ \left(\mathbf{p} - \frac{1}{2} \mathbf{k} \cos \theta \right)^2 + \left(\frac{1}{2} g_{\Sigma^-n} \mu \sin \theta \right)^2 \right\} - \mu \sin^2 \frac{\theta}{2} - \Sigma_{Kn} (1 - \cos \theta) \\
H_{n\Sigma^-} &= -\frac{i}{2} g_{\Sigma^-n} \sin \theta \left(\mathbf{k} - \frac{\mu}{M_N} \mathbf{p} \right) \cdot \boldsymbol{\sigma} = H_{\Sigma^-n}^* \\
H_{\Sigma^-\Sigma^-} &= \frac{1}{2M_N} \left\{ (\mathbf{p} + \frac{1}{2} \mathbf{k} \cos \theta)^2 + \left(\frac{1}{2} g_{\Sigma^-n} \mu \sin \theta \right)^2 \right\} + \delta M_{\Sigma^-N} - \mu \cos^2 \frac{\theta}{2} - \Sigma_{K\Sigma^-} (1 - \cos \theta) . \quad (7)
\end{aligned}$$

In Eq. (7), Σ_{KY} ($Y = \Lambda, \Sigma^-, \Xi^-$) are the “kaon-hyperon sigma terms” given by $\Sigma_{K\Lambda} \equiv -\left(\frac{5}{6}a_1 + \frac{5}{6}a_2 + 2a_3\right)(m_u + m_s)$, $\Sigma_{K\Sigma^-} = \Sigma_{Kn}$, and $\Sigma_{K\Xi^-} = \Sigma_{Kp}$. δM_{YN} ($Y = \Lambda, \Sigma^-, \Xi^-$) are the hyperon-nucleon mass difference. The p -wave axial vector coupling strengths are defined by $g_{\Lambda p} = (D+3F)/\sqrt{6}$ ($=0.87$), $g_{\Sigma^-n} = D-F$ ($=0.37$), and $g_{\Xi^-\Lambda} = (-D+3F)/\sqrt{6}$ ($=0.21$). For simplicity, the nucleon mass is taken to be the free neutron mass, $M_N = M_P = M_n = 939.57$ MeV, and the mass differences δM_{YN} are taken from the free baryon masses: $M_\Lambda = 1115.7$ MeV, $M_{\Sigma^-} = 1197.4$ MeV, and $M_{\Xi^-} = 1321.3$ MeV. The p -wave kaon-baryon Yukawa couplings are brought about through the terms proportional to $\mathbf{k} \cdot \boldsymbol{\sigma}$ with $\boldsymbol{\sigma}$ the spin matrix in the off-diagonal matrix elements in Eq. (7).

There appear terms of order $O(1/M_N)$ coming from meson-baryon recoils, $\mathbf{p} \cdot \mathbf{k}/M_N$, \mathbf{k}^2/M_N , $\mu \mathbf{p} \cdot \boldsymbol{\sigma}/M_N$, $\mu^2 \sin^2 \theta/M_N$, etc. in Eq. (7). The magnitude of the baryon momentum $|\mathbf{p}|$ is typically the Fermi momentum p_F , which is in the range $p_F \lesssim 4m_\pi$ with m_π being the pion mass. Thus these terms are considered to be small as compared with the kinetic energy $\mathbf{p}^2/(2M_N)$ of each baryon so long as $\mu = O(m_\pi)$ and $|\mathbf{k}| \lesssim 3m_\pi$. Numerically, these terms are not necessarily small. Nevertheless, we would like to elucidate mechanisms of kaon condensation within the basic p -wave kaon-baryon interaction in hyperonic matter, at the cost of detailed corrections to the effective Hamiltonian. Hence, for simplicity, we neglect the terms of order $O(M_N)$ except for the kinetic energy term.

After diagonalization of H_{eff}^B , the baryonic eigenstates are represented as “quasiparticles” which consist of superposition of the baryons, e.g., $|\tilde{p}\rangle = \alpha|p\rangle + \beta|\Lambda\rangle + \gamma|\Xi^-\rangle$, $|\tilde{n}\rangle = \delta|n\rangle + \epsilon|\Sigma^-\rangle$, etc., where $\alpha, \beta, \gamma, \delta, \epsilon$ are coefficients.⁷ The baryon contribution to the effective energy density, $\mathcal{E}_{\text{eff}}^B$, is obtained from occupation of the quasiparticles over each Fermi sea [65].

$$\mathcal{E}_{\text{eff}}^B = \sum_i \sum_{\substack{|\mathbf{p}| \leq |\mathbf{p}_F(i)| \\ s=\pm 1/2}} E_s^{(i)}(\mathbf{p}) , \quad (8)$$

where $\mathbf{p}_F(i)$ ($i = \tilde{p}, \tilde{\Lambda}, \tilde{\Xi}^-, \tilde{n}, \tilde{\Sigma}^-$) are the Fermi momenta, and the subscript ‘ s ’ stands for the spin states for the quasiparticles.

⁷ In general, the Σ^0 state is also superposed to the quasiparticle states $|\tilde{p}\rangle$, $|\tilde{\Lambda}\rangle$, and $|\tilde{\Xi}^-\rangle$ through the p -wave couplings, but we simply neglect the effects of the Σ^0 on these quasiparticle states.

The mesonic contribution to the effective energy density is given by the substitution of the classical kaon field (4) into $\mathcal{H}_{\text{eff}}^{\text{M}}$ as

$$\epsilon_{\text{eff}}^{\text{M}} = -\frac{1}{2}f^2(\mu^2 - \mathbf{k}^2)\sin^2\theta + f^2m_K^2(1 - \cos\theta) , \quad (9)$$

where $m_K \equiv [\Lambda_{\chi\text{SB}}(m_u + m_s)]^{1/2}$, which is identified with the free kaon mass, and is replaced by the experimental value, 493.7 MeV. The leptonic contribution in Eq. (5) reduces to the effective energy density

$$\epsilon_{\text{eff}}^e = \frac{\mu^4}{4\pi^2} - \mu\frac{\mu^3}{3\pi^2} = -\frac{\mu^4}{12\pi^2} \quad (10)$$

for the ultra-relativistic electrons. Thus one obtains the total effective energy density as $\mathcal{E}_{\text{eff}} = \mathcal{E}_{\text{eff}}^{\text{B}} + \mathcal{E}_{\text{eff}}^{\text{M}} + \mathcal{E}_{\text{eff}}^e$.

C. Potential contribution

Here we introduce baryon-baryon interactions beyond the framework of chiral symmetry. The potential energy density \mathcal{E}_{pot} produced from baryon-baryon interactions is crucial to obtaining the EOS and matter composition of the ground state for not only the normal (noncondensed) phase but also the condensed phase. We suppose that \mathcal{E}_{pot} depends on the extent of kaon condensation only implicitly through the change of each number density ρ_i ($i = p, \Lambda, \Xi^-, n, \Sigma^-$) due to condensation. Then the form of \mathcal{E}_{pot} is assumed to be $\mathcal{E}_{\text{pot}}(\rho_p, \rho_\Lambda, \rho_{\Xi^-}, \rho_n, \rho_{\Sigma^-})$. Following a procedure for incorporating nuclear interactions in case of pion condensation [68,69], we define the potential for the baryon V_i ($i=p, \Lambda, \Xi^-, n, \Sigma^-$) in hyperonic matter as

$$V_i = \partial\mathcal{E}_{\text{pot}}/\partial\rho_i , \quad (11)$$

which corresponds to a potential contribution to each baryon chemical potential, i.e., estimated at the Fermi momentum of each baryon. Thus momentum dependence of the potential is neglected, which is reasonable for the Σ^- and Λ potentials because of their weak momentum dependence, as suggested from recent microscopic calculations [47,48]. It should be reminded, however, that it is not a good approximation for the nuclear potentials where the potential depths at zero momentum are deeper than the value at the Fermi momentum.

The potential terms V_i are added to each diagonal matrix element of the baryonic part of the effective Hamiltonian $H_{\text{eff}}^{\text{B}}$ [Eq. (7)] as $H_{ii} \rightarrow H'_{ii} = H_{ii} + V_i$. Then the baryonic part of the modified effective energy density $\mathcal{E}'_{\text{eff}}^{\text{B}}$ is given by

$$\mathcal{E}'_{\text{eff}}^{\text{B}} = \sum_i \sum_{\substack{|\mathbf{p}| \leq |\mathbf{p}_F(i)| \\ s = \pm 1/2}} E'_s{}^{(i)}(\mathbf{p}) + \mathcal{E}_{\text{pot}} - \sum_{i=p,\Lambda,\Xi^-,n,\Sigma^-} \rho_i V_i , \quad (12)$$

where $E'_s{}^{(i)}(\mathbf{p})$ are eigenvalues diagonalized with inclusion of the V_i in the diagonal parts of $H_{\text{eff}}^{\text{B}}$. The last term on the r. h. s. in Eq. (12) is introduced in order to subtract the double counting of the baryon interaction energies in the first sum over the quasiparticle energies $E'_s{}^{(i)}(\mathbf{p})$.

For a practical use of the potential energy density \mathcal{E}_{pot} in hyperonic matter, we adopt the nonrelativistic expression by Balberg and Gal [49], which includes hyperon-hyperon interactions as well as hyperon-nucleon ones, and higher order terms in ρ_i simulating the many-body effects. The expression for the \mathcal{E}_{pot} is given in Appendix A. We take the exponents δ and γ in the density-dependent terms in Eq. (A1) to be $\delta = \gamma = 5/3$, which gives the moderate stiffness of the EOS among the three cases in Ref. [49]. Some of the parameters in \mathcal{E}_{pot} are refitted so as to be consistent with recent empirical data on nuclear and hypernuclear experiments and the saturation properties of symmetric nuclear matter: We take the saturation density $\rho_0=0.16 \text{ fm}^{-3}$, the binding energy 16 MeV, and the incompressibility 210 MeV at ρ_0 in symmetric nuclear matter, from which a_{NN} and c_{NN} are fixed for the isoscalar terms in the nucleon-nucleon (NN) part of the potential energy [Eq. (A1)]. From the symmetry energy $\sim 30 \text{ MeV}$ at $\rho_B = \rho_0$, one obtains b_{NN} for the isospin-dependent term for the NN part.⁸ For the ΛN part, $a_{\Lambda N}$ and $c_{\Lambda N}$ are taken to be the same as in Ref. [49]. The depth of the Λ potential in nuclear matter is then equal to the empirical value, i.e., V_Λ ($\rho_p = \rho_n = \rho_0/2$, $\rho_\Lambda = \rho_{\Xi^-} = \rho_{\Sigma^-} = 0$)= $a_{\Lambda N}\rho_0 + c_{\Lambda N}\rho_0^\gamma = -27 \text{ MeV}$ [72]. For the $\Xi^- N$ part, $a_{\Xi N}$ and $c_{\Xi N}$ are related with each other by the use of the depth of the Ξ^- potential in nuclear matter, which is deduced from the recent (K^-, K^+) experimental data as $-14 - -20 \text{ MeV}$ [73,74]. Here we put V_{Ξ^-} ($\rho_p = \rho_n = \rho_0/2$, $\rho_\Lambda = \rho_{\Xi^-} = \rho_{\Sigma^-} = 0$)= $a_{\Xi N}\rho_0 + c_{\Xi N}\rho_0^\gamma = -16 \text{ MeV}$. Further, the crossover density ρ_{co} , where $V_{\Xi^-}(\rho_B = \rho_{\text{co}}) = 0$, is taken to be equal to that for the Λ [49].

As for the V_{Σ^-} , recent (K^-, π^\pm) experiment at BNL [76] suggests a strong isospin dependence in the Σ -nucleus potential. It has been shown that the experimental data is compatible with the analysis by the Nijmegen model F for the baryon-baryon interaction, which gives a repulsive isoscalar part and a large positive isospin dependent term (Lane potential) for the Σ -nucleus potential [75]. The analysis of Σ^- atom data also shows the repulsive Σ^- potential [77]. Theoretically, a repulsive Σ potential in nuclear matter has been obtained from the G matrix calculation based on the SU(6) quark model baryon-baryon interaction [78]. Referring to these results, we first take the potential depth of the Σ^- in nuclear matter to be *repulsive* as follows: In Ref. [75], the Σ^- potential has been parametrized as $V_{\Sigma^-}(k_\Sigma) = V_0(k_\Sigma) - \frac{1}{2}V_1(k_\Sigma) \cdot \frac{2Z - A}{A}$, where k_{Σ^-} is the Σ^- momentum, and A , Z are the mass number and the atomic number, respectively. The calculated values in Ref. [75] for V_0 and V_1 at $k_\Sigma=0$ in nuclear matter based on the Nijmegen model F are identified with the correponding terms in our model such that

⁸ It is to be noted that the potential contribution $V_{\text{sym}}(\rho_B)$ to the symmetry energy is read from the isovector term for the NN interactions in Eq. (A1) as $V_{\text{sym}}(\rho_B) = b_{NN}\rho_B/2$, which mimics the density dependence of the $V_{\text{sym}}(\rho_B)$ in the RMF models. In normal neutron-star matter, this linear density dependence leads to a large proton fraction $\rho_p/\rho_B \gtrsim 0.1$ at high density and the large electron chemical potential μ_e through the relation $\mu_e = (3\pi^2\rho_e)^{1/3}$ and the charge neutrality $\rho_e = \rho_p$. The large proton fraction concerns with a possibility of the direct Urca process in neutron stars [70,71], and the large electron chemical potential assists the onset of the negatively charged hyperons, e.g., the Σ^- , through the chemical equilibrium condition, $\mu_n + \mu_e = \mu_{\Sigma^-}$ [51]. However, there is an ambiguity about the density dependence of the symmetry energy. E.g., the nonrelativistic potential models show its moderate increase in density in comparison with the RMF case [15,71].

$V_{\Sigma^-}(\rho_p = \rho_n = \rho_0/2, \rho_\Lambda = \rho_{\Xi^-} = \rho_{\Sigma^-} = 0) = a_{\Sigma N}\rho_0 + c_{\Sigma N}\rho_0^\gamma = V_0 = 23.5$ MeV, and $b_{\Sigma N}\rho_0 = V_1/2 = 40.2$ MeV. We call this parametrization for the repulsive Σ^- potential Case I. For the second case, the parameters $a_{\Sigma N}$, $b_{\Sigma N}$, and $c_{\Sigma N}$ are taken to be the same as in Ref. [49]. The depth of the V_{Σ^-} is then equal to that of the Λ as an extreme case for the attractive Σ^- potential, i.e., $a_{\Sigma N}\rho_0 + c_{\Sigma N}\rho_0^\gamma = -27$ MeV. We call this parametrization for the attractive Σ^- potential Case II.

The remaining parameters in the potential energy density \mathcal{E}_{pot} , relevant to the hyperon-hyperon interactions, are taken to be the same as those in Ref. [49]. The numerical values for the parameters are summarized in Tables I and II in Appendix A.

In general, there are additional off-diagonal matrix elements in $\mathcal{H}_{\text{eff}}^B$ in the presence of condensation. These off-diagonal matrix elements include the densities $\bar{\rho}_{p\Lambda} \equiv i\langle p^\dagger \boldsymbol{\sigma} \cdot \hat{\mathbf{k}}\Lambda \rangle$, $\bar{\rho}_{\Lambda\Xi^-} \equiv i\langle \Lambda^\dagger \boldsymbol{\sigma} \cdot \hat{\mathbf{k}}\Xi^- \rangle$, $\bar{\rho}_{n\Sigma^-} \equiv i\langle n^\dagger \boldsymbol{\sigma} \cdot \hat{\mathbf{k}}\Sigma^- \rangle$, where $\langle \dots \rangle$ means the ground state expectation value with $\hat{\mathbf{k}} \equiv \mathbf{k}/|\mathbf{k}|$. The strengths in these off-diagonal matrix elements are approximately related to the Landau-Migdal parameters, which simulate the short-range correlations between baryons, as is the case of pion condensation [68,69]. However, the values of the Landau-Migdal parameters for the particle-holes including hyperons are hardly known both theoretically and experimentally. Hence, in this paper, we don't take into account these extra off-diagonal matrix elements, by putting emphasis on a brief discussion about onset mechanisms of the p -wave kaon condensation within a simple model.

D. Kaon propagation in hyperonic matter

After expanding the total effective energy density $\mathcal{E}'_{\text{eff}}$ ($\equiv \mathcal{E}'_{\text{eff}}^B + \mathcal{E}_{\text{eff}}^M + \mathcal{E}_{\text{eff}}^e$) with respect to θ around $\theta = 0$ as $\mathcal{E}'_{\text{eff}} = \mathcal{E}'_{\text{eff}}(\theta = 0) - \frac{f^2}{2}D_K^{-1}(\mu, \mathbf{k}; \rho_B)\theta^2 + O(\theta^4)$, one obtains the kaon inverse propagator:

$$D_K^{-1}(\omega, \mathbf{k}; \rho_B) = \omega^2 - \mathbf{k}^2 - m_K^2 - \Pi_K(\omega, \mathbf{k}; \rho_B) \quad (13)$$

with the kaon self energy $\Pi_K(\omega, \mathbf{k}; \rho_B) = \Pi_K^s(\omega, \mathbf{k}; \rho_B) + \Pi_K^p(\omega, \mathbf{k}; \rho_B)$, where

$$\Pi_K^s(\omega, \mathbf{k}; \rho_B) = -\frac{1}{f^2} \sum_i \rho_i \Sigma_{Ki} - \frac{1}{f^2} \left(\rho_p + \frac{1}{2} \rho_n - \frac{1}{2} \rho_{\Sigma^-} - \rho_{\Xi^-} \right) \omega \quad (14a)$$

$$\begin{aligned} \Pi_K^p(\omega, \mathbf{k}; \rho_B) = & -\frac{1}{2f^2} \left[\frac{(\rho_p - \rho_\Lambda)(g_{\Lambda p}\mathbf{k})^2}{\delta M_{\Lambda p} - \omega + V_\Lambda - V_p} + \frac{(\rho_n - \rho_{\Sigma^-})(g_{\Sigma^- n}\mathbf{k})^2}{\delta M_{\Sigma^- n} - \omega + V_{\Sigma^-} - V_n} \right. \\ & \left. + \frac{(\rho_\Lambda - \rho_{\Xi^-})(g_{\Xi^- \Lambda}\mathbf{k})^2}{\delta M_{\Xi^- \Lambda} - \omega + V_{\Xi^-} - V_\Lambda} \right]. \end{aligned} \quad (14b)$$

The first term on the r.h.s. of Eq. (14a) gives the s -wave scalar attraction with ρ_i the number densities for baryons i ($i = p, \Lambda, \Xi^-, n, \Sigma^-$). The second term on the r.h.s. of Eq. (14a) gives the s -wave vector interaction, where the coefficients in front of the number densities come from the V -spin (\mathcal{V}_3). This term gives attraction for proton and neutron, while repulsion for Σ^- and Ξ^- . The p -wave part Π_K^p [Eq. (14b)] consists of the pole contributions from the p -wave kaon-baryon interaction. The diagrams corresponding to each term in Eq. (14b) are depicted in Fig. 1.⁹

⁹ The superscript ‘-1’ denotes a hole state.

The excitation energies for kaonic modes are obtained as zero points of the kaon inverse propagator, $D_K^{-1}(\omega, \mathbf{k}; \rho_B)$, which depends on the composition of the ground state of noncondensed hyperonic matter, i.e., the number densities for the particles, ρ_i ($i = p, \Lambda, \Xi^-, n, \Sigma^-, e^-$). The particle number densities are determined from charge neutrality condition, $\rho_p = \rho_{\Xi^-} + \rho_{\Sigma^-} + \rho_e$, baryon number conservation, $\rho_p + \rho_\Lambda + \rho_{\Xi^-} + \rho_n + \rho_{\Sigma^-} = \rho_B$, and chemical equilibrium conditions between p , Λ , Ξ^- , n , Σ^- and e^- ,

$$\mu_n = \mu_p + \mu_e \quad \text{for } n \rightleftharpoons pe^- \bar{\nu}_e , \quad (15a)$$

$$\mu_\Lambda = \mu_p + \mu_e \quad \text{for } pe^- \rightleftharpoons \Lambda \nu_e , \quad (15b)$$

$$\mu_{\Xi^-} = \mu_\Lambda + \mu_e \quad \text{for } \Lambda e^- \rightleftharpoons \Xi^- \nu_e , \quad (15c)$$

$$\mu_{\Sigma^-} = \mu_n + \mu_e \quad \text{for } ne^- \rightleftharpoons \Sigma^- \nu_e , \quad (15d)$$

where the chemical potentials for baryons μ_i are given by

$$\mu_i = (3\pi^2 \rho_i)^{2/3} / (2M_N) + \delta M_{iN} + V_i \quad (\delta M_{iN} = 0 \text{ for } i = p, n). \quad (16)$$

III. NUMERICAL RESULTS

A. K^- optical potential

We take a preliminary view of the in-medium kaon properties within our model by estimating a K^- optical potential $V_{\text{opt}}(\mathbf{k}; \rho_B)$ at $\rho_B = \rho_0$ in symmetric nuclear matter. The K^- optical potential $V_{\text{opt}}(\mathbf{k}; \rho_B)$ is defined in terms of the kaon self energy Π_K [Eq. (14)] as

$$V_{\text{opt}}(\mathbf{k}; \rho_B) = \Pi_{K^-}(\omega(\mathbf{k}, \rho_B), \mathbf{k}; \rho_B) / 2\omega(\mathbf{k}, \rho_B) , \quad (17)$$

where $\omega(\mathbf{k}, \rho_B)$ is the K^- excitation energy obtained from the dispersion equation, $D_K^{-1}(\omega, \mathbf{k}; \rho_B) = 0$ at given ρ_B and \mathbf{k} .

In Fig. 2, we show $V_{\text{opt}}(\mathbf{k}; \rho_0)$ as a function of the kaon momentum $|\mathbf{k}|$. The solid lines represent the total values coming from both the s and p -wave interactions [see Eq. (14)], and the dashed lines represent the contribution from the p -wave interaction. The bold lines are for $a_3 = -0.9$ ($\Sigma_{Kn}=305$ MeV), and the thin lines for $a_3 = -0.28$ ($\Sigma_{Kn}=0$). Since the numerical result depends little on the choice of the Σ^- potential (Case I or Case II), only Case I is shown in the figure. The total attractive potential energy decreases monotonically with \mathbf{k} . The potential depth at zero momentum is ~ -120 MeV for $a_3 = -0.9$ and ~ -55 MeV for $a_3 = -0.28$. It is to be noted that the total potential energy is attractive even if the s -wave scalar interaction is almost absent (thin solid line) due to the existence of the s -wave K^-N vector attraction (the Tomozawa-Weinberg term). Since the excitation energy for K^- is larger than those at the Σ^- and Λ poles, i.e., $\delta M_{\Sigma^-n} - \omega + V_{\Sigma^-} - V_n < 0$ and $\delta M_{\Lambda p} - \omega + V_\Lambda - V_p < 0$, the p -wave part of the optical potential is repulsive for K^- at this density, as seen from Eq. (14), and has a minor contribution in comparison with the s -wave attraction.

The K^- -nucleus potential has been obtained phenomenologically from kaonic atom data in several works. In Ref. [22], a strongly attractive potential inside a nucleus, Re

$V_{\text{opt}} = -200 \pm 20$ MeV, has been obtained with a nonlinear density dependent term. On the other hand, the energy shifts and widths have been well reproduced in Ref. [24] with much reduced attraction ~ -45 MeV in a local density approximation.

Several authors have elaborated the momentum-dependent K^- optical potential in nuclear matter. With a coupled channel approach based on chiral models [32,21], or a G -matrix method with the Jülich $\bar{K}N$ interaction [33] taking into account the in-medium modification of the kaon, they have obtained more moderate momentum dependence for $\text{Re } V_{\text{opt}}$ than ours over the relevant momentum region. On the other hand, our result for $a_3 = -0.9$ is similar to the result by a dispersion relation approach in Ref. [31]. At present, there is a controversy about the magnitude of the K^- potential at finite momentum as well as at zero momentum.

B. Particle fractions in hyperonic matter

Before considering the behaviors of kaonic modes, we make a survey of the ground state properties of hyperonic matter by obtaining the matter composition ρ_i ($i = p, n, \Lambda, \Sigma^-, \Xi^-, e^-$), which enters into the kaon self energy Eq. (14), being responsible for kaon dynamics. The particle fractions ρ_i/ρ_B as functions of the baryon number density ρ_B are shown in Fig. 3 (a) for Case I (the repulsive V_{Σ^-}) and Fig. 3 (b) for Case II (the attractive V_{Σ^-}).

In Case I, the Λ appears at $\rho_B \sim 0.37$ fm $^{-3}$, and its fraction rapidly increases with density, exceeding the proton fraction ($\rho_\Lambda > \rho_p$) at $\rho_B \sim 0.40$ fm $^{-3}$. Soon after the appearance of Λ , the Ξ^- are mixed at $\rho_B \sim 0.42$ fm $^{-3}$, and it increases with density. On the other hand, the electron fraction rapidly decreases after the appearance of the Λ and Ξ^- . The Σ^- does not appear over the relevant densities because of its repulsive potential.

In Case II, the Σ^- first appears at $\rho_B \sim 0.31$ fm $^{-3}$, and the Λ appears at $\rho_B \sim 0.40$ fm $^{-3}$ after the onset of Σ^- . Both fractions rapidly increase with density. In particular, the fraction of Λ exceeds the proton fraction at $\rho_B \sim 0.47$ fm $^{-3}$. The electron fraction decreases due to the appearance of the negatively charged hyperon Σ^- , which is qualitatively the same feature as for Case I. The electron chemical potential $\mu_e [= (3\pi^2 \rho_e)^{1/3}]$ also becomes small with increase in density, which is unfavorable to matching the chemical equilibrium condition, $\mu_{\Xi^-} = \mu_n + \mu_e$. Thus the existence region of the Ξ^- is pushed up to very high densities as compared with that in Case I.

These results for matter composition in Case I and II qualitatively reproduce the results of Figs. 4 and 3 in Ref. [49], respectively.

C. Kaonic modes in hyperonic matter

1. Case I (the repulsive V_{Σ^-})

(i) The weaker s -wave scalar interaction ($a_3 = -0.9$)

Here we discuss kaonic excitations in hyperonic matter in Case I. In Fig. 4 (a), we show the excitation energies for kaonic modes as functions of the kaon momentum $|\mathbf{k}|$ for $a_3 = -0.9$ ($\Sigma_{Kn}=305$ MeV) and $\rho_B=0.38$ fm $^{-3}$ in Case I. Around this density, the Λ begins

to appear in a neutron-star matter [Fig.3 (a)], where $\rho_\Lambda < \rho_p$. In addition to the K^- and K^+ branches, there are three particle-hole branches: Λp^{-1} , $\Xi^- \Lambda^{-1}$, and $\Sigma^- n^{-1}$. The excitation modes are discriminated by a sign of the residue $(\partial D_K^{-1}/\partial\omega)^{-1}$ at their pole of the Green's function D_K , as is the case with pionic modes [79–81]: If $\partial D_K^{-1}(\omega, \mathbf{k}; \rho_B)/\partial\omega > 0$, the mode has a K^- quantum number, while if $\partial D_K^{-1}(\omega, \mathbf{k}; \rho_B)/\partial\omega < 0$, the mode has a K^+ quantum number. In Fig. 4 (b), the value of the inverse kaon propagator D_K^{-1} is shown as a function of the excitation energy ω at $|\mathbf{k}|=500$ MeV for the same a_3 and density as Fig. 4 (a). The intersection with the ω axis denotes an excitation energy for each mode. One finds that the three particle-hole modes have the K^- quantum numbers at this density.

As is seen from Fig. 4 (a), the energies of the particle-hole branches depends little on the momentum $|\mathbf{k}|$, since the energy for each particle-hole mode is essentially determined from the location of the pole in the limit $|\mathbf{k}| \rightarrow 0$ in the p -wave part of the self energy (Eq. 14b), so long as the p -wave kaon-baryon coupling strength is not very strong. On the other hand, the energies of the K^+ and K^- branches are sensitive to $|\mathbf{k}|$.

Now we look into the behavior of the excitation modes at the higher density where the Λ is fully mixed and satisfies $\rho_\Lambda > \rho_p$. In Fig. 5 (a), we show the excitation energies for kaonic modes as functions of $|\mathbf{k}|$ for $a_3 = -0.9$ and $\rho_B=0.50$ fm $^{-3}$ (dashed lines) and $\rho_B=0.57$ fm $^{-3}$ (solid lines). The inset in Fig. 5 (a) shows the magnified part of the $p\Lambda^{-1}$ and $\Xi^- \Lambda^{-1}$ branches.

In Fig. 5 (b), the value of $D_K^{-1}(\omega, \mathbf{k}; \rho_B)$ as a function of ω at certain moentum $|\mathbf{k}|=k^C$ (=984 MeV) is shown for the same a_3 and ρ_B as in Fig. 5 (a). For these high densities, the $p\Lambda^{-1}$ branch which has a quantum number of the K^+ appears instead of the Λp^{-1} branch: E.g., for $\rho_B=0.50$ fm $^{-3}$, $\partial D_K^{-1}/\partial\omega < 0$ at the pole of the $p\Lambda^{-1}$ mode [Fig. 5 (b)]. In order to go into details about the condition for the appearance of the $p\Lambda^{-1}$ mode, one obtains from Eqs.(13) and (14),

$$\begin{aligned} \partial D_K^{-1}/\partial\omega = 2\omega + \frac{1}{f^2} & \left[\left(\rho_p + \frac{1}{2}\rho_n - \frac{1}{2}\rho_{\Sigma^-} - \rho_{\Xi^-} \right) + \frac{1}{2}(\rho_p - \rho_\Lambda) \left(\frac{g_{\Lambda p}\mathbf{k}}{\delta M_{\Lambda p} - \omega + V_\Lambda - V_p} \right)^2 \right. \\ & + \frac{1}{2}(\rho_\Lambda - \rho_{\Xi^-}) \left(\frac{g_{\Xi^- \Lambda}\mathbf{k}}{\delta M_{\Xi^- \Lambda} - \omega + V_{\Xi^-} - V_\Lambda} \right)^2 \\ & \left. + \frac{1}{2}(\rho_n - \rho_{\Sigma^-}) \left(\frac{g_{\Sigma^- n}\mathbf{k}}{\delta M_{\Sigma^- n} - \omega + V_{\Sigma^-} - V_n} \right)^2 \right]. \end{aligned} \quad (18)$$

Since the excitation energy $\omega(p\Lambda^{-1})$ for the $p\Lambda^{-1}$ mode roughly satisfies $\delta M_{\Lambda p} - \omega(p\Lambda^{-1}) + V_\Lambda - V_p \sim 0$, the second term in the bracket on the r.h.s. of Eq. (18) coming from the $K^- p\Lambda$ interaction is dominant, and a sum of the remaining terms in (18) is positive. Hence, in order to satisfy $\partial D_K^{-1}/\partial\omega < 0$, the Λ have to be more abundant than the proton ($\rho_\Lambda > \rho_p$), which is the necessary (but not sufficient) condition for the existence of the $p\Lambda^{-1}$ mode. In Case I, the $p\Lambda^{-1}$ mode appears at $\rho_B \sim 0.40$ fm $^{-3}$, where $\rho_p \simeq \rho_\Lambda$ [see Fig. 3].

As the baryon number density increases, the locations of the particle-hole branches become lower owing to the p -wave interactions, as shown in Fig. 5 (a). In particular, the $\Xi^- \Lambda^{-1}$ and $p\Lambda^{-1}$ branches get close to each other, and they merge at certain density ($\rho_B \simeq 0.57$ fm $^{-3}$) with a critical momentum k^C (=984 MeV). At $|\mathbf{k}| = k^C$, these two excitation modes merge at the ω axis in the $D_K^{-1} - \omega$ plane [Fig. 5 (b)], where the double-pole

condition,

$$D_K^{-1}(\omega, \mathbf{k}; \rho_B) = 0 , \quad (19a)$$

$$\partial D_K^{-1}(\omega, \mathbf{k}; \rho_B) / \partial \omega = 0 , \quad (19b)$$

and the extremum condition with respect to $|\mathbf{k}|$,

$$\partial D_K^{-1}(\omega, \mathbf{k}; \rho_B) / \partial |\mathbf{k}| = 0 , \quad (20)$$

are satisfied. It means that a pair of the two modes, $\Xi^-\Lambda^{-1}$ and $p\Lambda^{-1}$, are created spontaneously with no cost of energy because the energy of $p\Lambda^{-1}$ mode with the quantum number K^+ is to be reversed in sign. Hence the system is unstable with respect to a pair creation of $[\Xi^-\Lambda^{-1}]$ and $[p\Lambda^{-1}]$ modes. This instability originates from the p -wave kaon-baryon interaction, and we call this instability p -wave kaon condensation. The onset mechanism of the p -wave kaon condensation is similar to that of pion condensation, where a driving force is given by the p -wave πN interaction [79–82].

From Eqns. (19a), (19b), (20), and by putting $\omega = \mu$ (the charge chemical potential), one obtains the baryon number density ρ_B^C , the charge chemical potential μ^C , and the kaon momentum k^C at the onset of condensation.

The effects of the p -wave kaon-baryon interaction on the kaon dynamics near the onset density of condensation are evaluated from the self energy Π_K . For each kaonic mode, we show, in Fig. 6, the kaon self energy for the s -wave part $\Pi_K^s(\omega, \mathbf{k}; \rho_B)$ [Eq. (14a)] and the p -wave part $\Pi_K^p(\omega, \mathbf{k}; \rho_B)$ [Eq. (14b)] by the dashed lines and the solid lines, respectively, as a function of $|\mathbf{k}|$ for $a_3 = -0.9$ and $\rho_B = \rho_B^C = 0.57 \text{ fm}^{-3}$. For the $p\Lambda^{-1}$, Σ^-n^{-1} , and $\Xi^-\Lambda^{-1}$, the attractive p -wave part Π_K^p gets large almost proportionally to $|\mathbf{k}|^2$, and the magnitude becomes comparable to that of the s -wave part Π_K^s at $|\mathbf{k}| \sim 500 \text{ MeV}$.

On the other hand, the p -wave part Π_K^p for the K^- works repulsively at small $|\mathbf{k}|$, and it decreases monotonically with $|\mathbf{k}|$. At a high momentum, the excitation energy for the K^- mode is so large that the K^- mode is located far beyond the poles for the other particle-hole modes, which yields $\delta M_{\Lambda p} - \omega(K^-) + V_\Lambda - V_p \ll 0$, $\delta M_{\Sigma^-n} - \omega(K^-) + V_{\Sigma^-} - V_n \ll 0$, and $\delta M_{\Xi^-\Lambda} - \omega(K^-) + V_{\Xi^-} - V_\Lambda \ll 0$ in the Π_K^p . Hence the magnitude of the p -wave part Π_K^p for the K^- is tiny, and the s -wave part Π_K^s is dominant in the self energy.

(ii) The stronger s -wave scalar interaction ($a_3 = -1.1$)

Next we consider a case for the stronger s -wave scalar attraction. In Fig. 7 (a), we show the excitation energies of kaonic modes as functions of $|\mathbf{k}|$ for $a_3 = -1.1$ ($\Sigma_{Kn} = 403 \text{ MeV}$) and $\rho_B = 0.48 \text{ fm}^{-3}$ just beyond the onset of condensation. In Fig. 7 (b), the value of the kaon inverse propagator $D_K^{-1}(\omega, \mathbf{k}; \rho_B)$ is shown as a function of ω at $|\mathbf{k}| = k^C = 118 \text{ MeV}$ for the same values of a_3 and ρ_B as those in Fig. 7 (a). As is the case with $a_3 = -0.9$, the p -wave condensation of the $[\Xi^-\Lambda^{-1}]$ and $[p\Lambda^{-1}]$ pairs occurs but at a smaller density $\rho_B = 0.48 \text{ fm}^{-3}$ and a smaller momentum $|\mathbf{k}|^C = 118 \text{ MeV}$ than those for $a_3 = -0.9$. The difference of the critical density and the critical momentum between the two cases is attributed to the difference of the microscopic structures of the kaonic modes. Figure 7 (a) shows that there are level crossings between the K^- , Σ^-n^{-1} and $\Xi^-\Lambda^{-1}$ branches, whereas there is a level crossing only between the K^- and Σ^-n^{-1} branches for $a_3 = -0.9$ [Fig. 5 (a)]. The difference of the structures for the kaonic modes between the $a_3 = -0.9$ and -1.1

cases can also be seen from the dependence of the kaonic modes on the baryon number density. In Figs. 8, we show the dependence of the excitation energies of kaonic modes on the baryon number density except for the K^+ . (a) is for $a_3 = -0.9$ and $|\mathbf{k}|=500$ MeV which is smaller than k^C ($=984$ MeV), and (b) is for $a_3 = -1.1$ and $|\mathbf{k}|=100$ MeV, which is smaller than but near k^C ($=118$ MeV). For $a_3 = -0.9$, the K^- is repelled far from the remaining particle-hole modes over the relevant densities, and there is no level crossing. The $\Xi^- \Lambda^{-1}$ and $p\Lambda^{-1}$ modes merge at $\rho_B \simeq 0.60$ fm $^{-3}$, which corresponds to the instability with respect to p -wave condensation. The qualitative feature is also applied to the case at the critical momentum k^C which satisfies the conditions Eqs. (19) and (20). The particle-hole branches such as the $\Xi^- \Lambda^{-1}$ and $p\Lambda^{-1}$ do not depend much on the value of $|\mathbf{k}|$, nor does the critical point for the p -wave condensation.

For $a_3 = -1.1$, on the other hand, the excitation energy of the K^- is small as compared with the $a_3 = -0.9$ at a given density due to the larger s -wave scalar attraction and the smaller momentum $|\mathbf{k}|$, and one can see in Fig. 8 (b) that there are energy gaps between K^- and $\Sigma^- n^{-1}$ branches and the $\Sigma^- n^{-1}$ and $\Xi^- \Lambda^{-1}$ branches owing to the level crossings.¹⁰ As a result of the level crossings, the $\Xi^- \Lambda^{-1}$ branch takes over the characteristics of the K^- , the excitation energy of which changes appreciably depending on the magnitude of the s -wave scalar interaction simulated by a_3 .¹¹ Thus, when the level crossing occurs, the behavior of the $\Xi^- \Lambda^{-1}$ branch is sensitive to the value of a_3 , and the critical point for the p -wave condensation, which is given by the merge point of the $\Xi^- \Lambda^{-1}$ and $p\Lambda^{-1}$ branches, also depends on a_3 . This mechanism of p -wave condensation is similar to that of p -wave pion condensation, where the π^- mode, which reduces to a free π^- in vacuum, and the spin-isospin zero sound (called π_s^+) are spontaneously created in pairs [79–82].

The larger mixing of the Λ than the proton in hyperonic matter is crucial to the realization of p -wave kaon condensation. The result should be compared with a mechanism of p -wave kaon condensation realized from the conventional neutron-star matter where only the nucleons n, p are present as baryons [58]. In the latter case, the Bose-Einstein condensation of the K^- precedes at a lower density as a result of the s -wave $K^- N$ attraction, and at a higher density, the classical K^- field simply acquires a momentum smoothly from zero, amplifying the energy gain of the system due to the p -wave kaon-baryon interaction [58].

As seen in Fig. 8, the Λp^{-1} branch crosses the charge chemical potential, i. e., $\omega(\Lambda p^{-1}) = \mu$ at $\rho_B \sim 0.40$ fm $^{-3}$. It apparently suggests an onset of another type of Bose-Einstein condensation of Λp^{-1} mode. In Fig. 9, we show the occupation factors $\Gamma(i)$ which are defined as $\Gamma(i) \equiv 2\omega(\partial D_K^{-1}/\partial\omega)^{-1}|_{\omega=\omega_i}$ [59] for the kaonic modes ($i = K^-, \Lambda p^{-1}, \Sigma^- n^{-1}, \Xi^- \Lambda^{-1}$) as functions of $|\mathbf{k}|$ for $a_3 = -0.9$ and $\rho_B = 0.38$ fm $^{-3}$ in Case I. The value of Γ for the Λp^{-1} mode as well as the $\Xi^- \Lambda^{-1}$ is negligible over the relevant kaon momentum $|\mathbf{k}|$, and the K^- and $\Sigma^- n^-$ modes have dominant contribution. Hence we consider this crossing point as irrelevant to an actual instability of the system.

¹⁰The appearance of the collective modes was also pointed out in relation to the level crossing in Ref. [61].

¹¹This mode corresponds to the kaesobar [26,57].

2. Case II (the attractive V_{Σ^-})

Next we discuss behaviors of kaonic modes in Case II (the attractive V_{Σ^-}). In Fig. 10, we show the dependence of the excitation energies of kaonic modes on the baryon number density in Case II. (a) is for $a_3 = -0.9$ ($\Sigma_{Kn}=305$ MeV) and $|\mathbf{k}|=500$ MeV, and (b) is for $a_3 = -1.1$ ($\Sigma_{Kn}=403$ MeV) and $|\mathbf{k}|=30$ MeV. Due to the strong attraction of V_{Σ^-} , the $\Sigma^- n^{-1}$ branch is softer than those of the $\Xi^- \Lambda^{-1}$ and K^- branches for $\rho_B \gtrsim 0.40$ fm $^{-3}$, and the $\Sigma^- n^{-1}$ merges first with the $p\Lambda^{-1}$ branch instead of the $\Xi^- \Lambda^{-1}$. Hence, in Case II, p -wave condensation is brought about by a spontaneous creation of the $\Sigma^- n^{-1}$ and $p\Lambda^{-1}$ pair. For the larger a_3 [Fig. 10 (b)], there are level crossings between the K^- , $\Sigma^- n^{-1}$ and $\Xi^- \Lambda^{-1}$. The $\Sigma^- n^{-1}$ branch takes over the characteristics of the K^- around the crossing point with the $\Xi^- \Lambda$ branch [$\rho_B \sim 0.53$ fm $^{-3}$], so that the critical point for the p -wave condensation is sensitive to the value of a_3 , which is similar to the stronger s -wave attraction case ($a_3 = -1.1$) in Case I [see Fig. 8 (b)].

The critical density and the corresponding momentum are given from Eq. (20) in addition to the double-pole condition Eq. (19) as $\rho_B^C=0.64$ fm $^{-3}$, $k^C=978$ MeV for $a_3 = -0.9$, and $\rho_B^C=0.53$ fm $^{-3}$, $k^C=39$ MeV for $a_3 = -1.1$. Quantitatively, the critical density in Case II is a little larger than that in Case I. This difference comes from a property of the Σ^- potential, which affects the density dependence of the relevant kaonic modes through changing chemical composition of highly dense matter.

3. Comparison of the critical densities for p -wave and s -wave condensations

Here we compare the critical density for the p -wave condensation discussed in the preceding subsections with that for the s -wave K^- condensation which is obtained within the present framework. In Fig. 11, we show the dependence of the minimum excitation energy of the s -wave K^- on the baryon number density for $|\mathbf{k}| = 0$ in Case I. The solid line is for $a_3 = -0.9$ and the dashed line is for $a_3 = -1.1$. The K^- energy decreases with density due to the s -wave kaon-baryon interaction in Π_K^s [Eq. (14a)]. However, due to the substantial decrease of the charge chemical potential μ with density in the presence of hyperons, the onset condition for the s -wave K^- condensation, $\omega_{\min}(K^-) = \mu$, is met at a much larger density (filled circles) than that in the conventional neutron-star matter which consists of only the nucleons n , p and e^- . On the other hand, the critical density of the p -wave condensation is indicated by the arrows in Fig. 11 (the solid arrow for $a_3 = -0.9$ and the dashed arrow for $a_3 = -1.1$). One finds that the p -wave condensation precedes the s -wave K^- condensation.

In Fig. 12, we summarize the dependence of the critical density of the p -wave kaon condensation $\rho_B^C(p)$ (solid and dotted lines) on the kaon-neutron sigma term Σ_{Kn} [$\equiv -(a_2+2a_3)(m_u+m_s)$]. For comparison, the critical density of the s -wave K^- condensation $\rho_B^C(s)$ (the dashed line) is also shown. (a) is for Case I and (b) is for Case II. For the strong s -wave scalar attraction such that $\Sigma_{Kn} \gtrsim 340$ MeV ($a_3 \lesssim -0.98$), there are level crossings between the K^- and the particle-hole branches. As a result, the critical density $\rho_B^C(p)$ is sensitive to the magnitude of $|a_3|$. $\rho_B^C(p)$ is slightly larger than $\rho_B^C(s)$ in both Cases I

and II, but the difference is small, as shown by the dotted lines and dashed lines. For the weaker s -wave attraction such that $\Sigma_{Kn} \lesssim 340$ MeV ($a_3 \gtrsim -0.98$), the critical density of the p -wave condensation $\rho_B^C(p)$ depends little on the magnitude of a_3 (the solid lines). This is because the $p\Lambda^{-1}$, $\Xi^-\Lambda^{-1}$, and Σ^-n^{-1} branches hardly depend on the magnitude of a_3 as long as no level crossing with the K^- branch occurs before the onset of instability. The critical density $\rho_B^C(p)$ changes little over the range from $\Sigma_{Kn}=0$ ($a_3 = -0.28$) to $\Sigma_{Kn} \sim 340$ MeV ($a_3 \sim -0.98$) in both Cases I and II. On the other hand, the critical density for the s -wave K^- condensation $\rho_B^C(s)$ becomes large as Σ_{Kn} (or $|a_3|$) becomes small, due to the reduced contribution from the s -wave scalar attraction to the K^- excitation energy $\omega(K^-)$. In conclusion, the critical density of the p -wave condensation is always smaller than that of the s -wave K^- condensation as long as $|a_3|$ is not too large, and the difference between these critical densities gets remarkable with the decrease in the magnitude of the s -wave scalar attraction.

IV. SUMMARY AND CONCLUDING REMARKS

We have discussed in-medium properties of kaonic modes in hyperonic matter by taking into account the p -wave kaon-baryon interaction as well as the s -wave one on the basis of chiral symmetry. Nonrelativistic effective baryon-baryon interactions, which are parametrized by the use of the recent hypernuclear experimental data, have been used. It has been shown that a collective $p\Lambda^{-1}$ mode with the K^+ quantum number appears over the densities where the Λ is more abundant than the proton. The system becomes unstable with respect to a creation of $[\Xi^-\Lambda^{-1}]$ and $[p\Lambda^{-1}]$ pair or $[\Sigma^-n^{-1}]$ and $[p\Lambda^{-1}]$ pair (p -wave kaon condensation), which stems from the p -wave kaon-baryon interaction. The onset density of this instability is lower than that of the s -wave K^- condensation for a standard value of the parameter a_3 simulating the magnitude of the s -wave kaon-baryon scalar interaction, and it hardly depends on the value of a_3 as long as $|a_3|$ is not too large.

The possibility of the p -wave kaon condensation depends on composition of baryons in hyperonic matter. In particular, large mixing of Λ as compared with that of the proton is needed for the appearance of the $p\Lambda^{-1}$ mode. The details about the onset densities of hyperons and their fractions at high densities differ between specific models for the baryonic potentials. One of the important ingredients which control matter composition is three-body forces for baryons [47,51]. It has been shown that phenomenological inclusion of three-body forces for only nucleons makes hyperon-mixing favorable [47]. However, it has been pointed out that inclusion of three-body forces for hyperons on the same footing as the nucleons may considerably change the results on the matter composition and the resultant EOS of the hyperonic matter [51]. Thus one has to be careful for the parametrization of the effective baryon-baryon interactions used in this paper, keeping consistency with these other model calculations.

Our model used for the p -wave kaon-baryon interaction is based on the leading order expansion in the chiral perturbation theory. Higher order terms in chiral expansion which are relevant to the p -wave meson-baryon scatterings have been estimated with reference to the experimental results such as pion and photon-induced reactions [66] or elastic and inelastic K^-p scatterings [67]. It needs more consideration whether these higher order terms are quantitatively important to kaon dynamics in highly dense matter.

It has to be elucidated whether the instability of the system with respect to the p -wave condensation leads to a fully condensed phase beyond the critical density. In this context, the EOS of the p -wave condensed phase and the characteristic features of the system have to be examined [65]. Mixing of hyperons only already leads to appreciable softening of the EOS [42,46–55]. Hence, further development of kaon condensates in hyperonic matter would make the EOS too soft to obtain the observed neutron star masses $\sim 1.4M_{\odot}$ [83,84] or even much larger masses $\sim 2.0M_{\odot}$ if the recent analyses from the observations of the quasi-periodic oscillations (QPO) [85] are confirmed [48]. Relativistic effects may help weaken the softness of the EOS, since it has been shown that the energy gain of kaon condensation coming from the s -wave scalar attraction is suppressed by relativistic effects [8,4]: As a kaon condensate develops, the effective nucleon mass M^* decreases due to the scalar attraction, which leads to suppression of the scalar density, $\rho_s = \int \frac{d^3p}{(2\pi)^3} M^* / \sqrt{\mathbf{p}^2 + M^{*2}}$. Thus the energy gain of the condensed phase from the scalar attraction ($\propto \rho_s \Sigma_{KN}$ with the KN sigma term Σ_{KN}) and the growth of a condensate are suppressed.

In addition, in view of making the EOS consistent with observations, some realistic effects which reduce the p -wave kaon-baryon attraction should be taken into account: (1) vertex renormalization at the p -wave kaon-baryon vertices in terms of form factors. (2) short-range correlations between baryons. For the p -wave part, the off-diagonal matrix elements in the baryonic part of the effective Hamiltonian [Eq. (6)] are to be added by the particle-hole densities, the strengths of which are related with the Landau-Migdal parameters in the relevant channel in the same way as pion condensation [68,79–82].

We have not taken into account the effects of the other subthreshold resonances such as $\Sigma(1385)$ (abbreviated to Σ^*) on the dispersion relations of the kaonic modes. However, the excitation energies of the $\Sigma^* N^{-1}$ modes are of the order ~ 450 MeV so that their branches lie far above the other particle-hole branches, $p\Lambda^{-1}$, $\Sigma^- n^{-1}$, $\Xi^- \Lambda^{-1}$ considered in this paper. Furthermore, their coupling strengths $g_{\Sigma^* N}$ to the $K^- N$ are not so large as compared with $g_{\Lambda p}$, $g_{\Sigma^- n}$, and $g_{\Xi^- \Lambda}$. Hence the inclusion of these resonances would not change the results quantitatively.

V. ACKNOWLEDGEMENTS

The author would like to thank T. Tatsumi for useful discussions and comments. The author is also grateful to T. Takatsuka, S. Nishizaki, M. Yasuhira, D. N. Voskresensky, J. Schaffner-Bielich and P. K. Sahu for discussions and interest in this work. This work is supported in part by the Japanese Grant-in-Aid for Scientific Research Fund (C) of the Ministry of Education, Science, Sports, and Culture (No. 12640289). Numerical calculations were carried out on the DEC Alpha Server 4100 System, Chiba Institute of Technology.

APPENDIX A: POTENTIAL ENERGY DENSITY IN HYPERONIC MATTER

We show the expression for the potential energy density \mathcal{E}_{pot} based on the nonrelativistic baryon-baryon interactions by Balberg and Gal (Eq. (6) in [49]). Since only p , Λ , Ξ^- , n ,

and Σ^- are incorporated for the baryons in this paper, the other terms relevant to Σ^0 , Σ^+ , and Ξ^0 are omitted.

$$\begin{aligned}
\mathcal{E}_{\text{pot}} = & \frac{1}{2} \left[a_{\text{NN}}(\rho_p + \rho_n)^2 + b_{\text{NN}}(\rho_p - \rho_n)^2 + c_{\text{NN}}(\rho_p + \rho_n)^{\delta+1} \right] \\
& + a_{\Lambda N}(\rho_p + \rho_n)\rho_\Lambda + c_{\Lambda N} \left[\frac{(\rho_p + \rho_n)^{\gamma+1}}{\rho_p + \rho_n + \rho_\Lambda} \rho_\Lambda + \frac{\rho_\Lambda^{\gamma+1}}{\rho_p + \rho_n + \rho_\Lambda} (\rho_p + \rho_n) \right] \\
& + \frac{1}{2} \left[a_{YY}\rho_\Lambda^2 + c_{YY}\rho_\Lambda^{\gamma+1} + (a_{YY} + b_{\Xi\Xi})\rho_{\Xi^-}^{-2} + c_{YY}\rho_{\Xi^-}^{-\gamma+1} \right] \\
& + a_{\Xi N}(\rho_p + \rho_n)\rho_{\Xi^-} + b_{\Xi N}(\rho_n - \rho_p)\rho_{\Xi^-} \\
& + c_{\Xi N} \left[\frac{(\rho_p + \rho_n)^{\gamma+1}}{\rho_p + \rho_n + \rho_{\Xi^-}} \rho_{\Xi^-} + \frac{\rho_{\Xi^-}^{\gamma+1}}{\rho_p + \rho_n + \rho_{\Xi^-}} (\rho_p + \rho_n) \right] \\
& + a_{YY}\rho_{\Xi^-}\rho_\Lambda + c_{YY} \left[\frac{\rho_\Lambda^{\gamma+1}}{\rho_{\Xi^-} + \rho_\Lambda} \rho_{\Xi^-} + \frac{\rho_{\Xi^-}^{\gamma+1}}{\rho_{\Xi^-} + \rho_\Lambda} \rho_\Lambda \right] \\
& + a_{\Sigma N}(\rho_p + \rho_n)\rho_{\Sigma^-} + b_{\Sigma N}(\rho_n - \rho_p)\rho_{\Sigma^-} \\
& + c_{\Sigma N} \left[\frac{(\rho_p + \rho_n)^{\gamma+1}}{\rho_p + \rho_n + \rho_{\Sigma^-}} \rho_{\Sigma^-} + \frac{\rho_{\Sigma^-}^{\gamma+1}}{\rho_p + \rho_n + \rho_{\Sigma^-}} (\rho_p + \rho_n) \right] \\
& + a_{YY}\rho_{\Sigma^-}\rho_\Lambda + c_{YY} \left[\frac{\rho_{\Sigma^-}^{\gamma+1}}{\rho_{\Sigma^-} + \rho_\Lambda} \rho_\Lambda + \frac{\rho_\Lambda^{\gamma+1}}{\rho_{\Sigma^-} + \rho_\Lambda} \rho_{\Sigma^-} \right] \\
& + a_{YY}\rho_{\Sigma^-}\rho_{\Xi^-} + b_{\Sigma\Xi}\rho_{\Xi^-}\rho_{\Sigma^-} + c_{YY} \left[\frac{\rho_{\Xi^-}^{\gamma+1}}{\rho_{\Xi^-} + \rho_{\Sigma^-}} \rho_{\Sigma^-} + \frac{\rho_{\Sigma^-}^{\gamma+1}}{\rho_{\Xi^-} + \rho_{\Sigma^-}} \rho_{\Xi^-} \right] \\
& + \frac{1}{2} \left[(a_{YY} + b_{\Sigma\Sigma})\rho_{\Sigma^-}^{-2} + c_{YY}\rho_{\Sigma^-}^{-\gamma+1} \right]
\end{aligned} \tag{A1}$$

The parameters relevant to the NN and YN parts in Eq. (A1) have been refitted in reference to the recent empirical data on the nuclear and hypernuclear properties. Numerical values of the parameters are listed in Tables I and II.

REFERENCES

- [1] D. B. Kaplan and A. E. Nelson, Phys. Lett. **B175** (1986) 57; **179** (1986) 409(E).
- [2] C. -H. Lee, G. E. Brown, D. -P. Min and M. Rho, Nucl. Phys. **A 585** (1995) 401.
- [3] For a review, T. Tatsumi, Prog. Theor. Phys. Suppl. **120** (1995) 111.
- [4] H. Fujii, T. Maruyama, T. Muto and T. Tatsumi, Nucl. Phys. **A597** (1996) 645 .
- [5] C. -H. Lee, Phys. Rep. **275** (1996) 197 .
- [6] M. Prakash, I. Bombaci, M. Prakash, P. J. Ellis, J. M. Lattimer, R. Knorren, Phys. Rep. **280** (1997) 1.
- [7] V. Thorsson, M. Prakash and J. M. Lattimer, Nucl. Phys. **A 572** (1994), 693 ; *ibid* **A 574** (1994), 851 (E).
- [8] T. Maruyama, H. Fujii, T. Muto and T. Tatsumi, Phys. Lett. **B 337** (1994) 19.
- [9] N. K. Glendenning and J. Schaffner-Bielich, Phys. Rev. Lett. **81** (1998) 4564 ; Phys. Rev. **C60** (1999) 025803 .
- [10] T. Tatsumi and M. Yasuhira, Nucl. Phys. **A 653** (1999) 133; *ibid* **A 670** (2000) 218; M. Yasuhira and T. Tatsumi, Nucl. Phys. **A 663** (2000) 881c.
- [11] J. A. Pons, S. Reddy, P. J. Ellis, M. Prakash and J. M. Lattimer, Phys. Rev. **C 62** (2000) 035803.
- [12] G. E. Brown, K. Kubodera, D. Page and P. Pizzecherro, Phys. Rev. **D37** (1988) 2042 .
- [13] T. Tatsumi, Prog. Theor. Phys. **80** (1988) 22 .
- [14] D. Page and E. Baron, Astrophys. J. **254** (1990) L17.
- [15] H. Fujii, T. Muto, T. Tatsumi and R. Tamagaki, Nucl. Phys. **A571**, 758 (1994); Phys. Rev. **C50** (1994) 3140.
- [16] T. Waas, M. Rho and W. Weise, Nucl. Phys. **A 617** (1997) 449.
- [17] J. Carlson, H. Heiselberg and V. R. Pandharipande, Phys. Rev. **C 63** (2000) 017603.
- [18] V. Koch, Phys. Lett. **B337** (1994) 7 .
- [19] T. Waas, N. Kaiser and W. Weise, Phys. Lett. **B365** (1996) 12 ; **B379** (1996) 34 .
T. Waas and W. Weise, Nucl. Phys. **A625** (1997) 287.
- [20] M. Lutz, Phys. Lett. **B426** (1998) 12 .
- [21] A. Ramos and E. Oset, Nucl. Phys. **A 671** (2000) 481.
- [22] E. Friedman, A. Gal and C. J. Batty, Nucl. Phys. **A 579** (1994) 518;
C. J. Batty, E. Friedman and A. Gal, Phys. Rep. **287** (1997) 385.
- [23] E. Friedman, A. Gal, J. Mares and A. Cieply, Phys. Rev. **C 60** (1999) 024314.
- [24] S. Hirenzaki, Y. Okumura, H. Toki, E. Oset and A. Ramos, Phys. Rev. **C 61** (2000) 055205.
- [25] A. Baca, C. Garcia-Recio and J. Nieves, Nucl. Phys. **A 673** (2000) 335.
- [26] G. Q. Li, C.- H. Lee and G. E. Brown, Phys. Rev. Lett. **79** (1997) 5214 ; Nucl. Phys. **A625** (1997) 372.
- [27] C. M. Ko and G. Q. Li, J. Phys. **G 22** (1996) 1673.
- [28] G. Song, B.- A. Li and C. M. Ko, Nucl. Phys. **A646** (1999) 481.
- [29] J. Schaffner-Bielich, I. N. Mishustin and J. Bondorf, Nucl. Phys. **A625** (1997) 325 .
- [30] W. Cassing and E. L. Bratkovskaya, Phys. Rep. **308** (1999) 65 .
- [31] A. Sibirtsev and W. Cassing, Nucl. Phys. **A 641** (1998) 476; nucl-th/9909024.
- [32] J. Schaffner-Bielich, V. Koch and M. Effenberger, Nucl. Phys. **A 669** (2000) 153.
- [33] L. Tolós, A. Ramos, A. Polls and T. T. S. Kuo, nucl-th/0007042.
- [34] R. Barth et al., Phys. Rev. Lett. **78** (1997) 4007.
- [35] F. Laue et al., Phys. Rev. Lett. **82** (1999) 1640.
- [36] For a review, P. Senger and H. Ströbele, J. Phys. **G25** (1999) R59.
- [37] T. Kishimoto, Phys. Rev. Lett. **83** (1999) 4701.

[38] Y. Akaishi, Proceedings of the VII International Conference on Hypernuclear and Strange Particle Physics, Torino, Italy, October 23-27,2000, to be published in Nucl. Phys. **A**; M. Iwasaki, *ibid.*

[39] S. Tsuruta and A. G. W. Cameron, Can. J. Phys. **44** (1966) 1895.

[40] W. D. Langer and L. Rosen, Astrophys. Space Sci. **6** (1970) 217.

[41] V. R. Pandharipande, Nucl. Phys. **A 178** (1971) 123.

[42] N. K. Glendenning, Astrophys. J. **293** (1985) 470 ; Phys. Rev. Lett. **81** (1998) 2176 , and references therein.

[43] P. J. Ellis, R. Knorren, and M. Prakash, Phys. Lett. **B349** (1995) 11 .
R. Knorren, M. Prakash and P. J. Ellis, Phys. Rev. **C52** (1995) 3470.

[44] J. Schaffner and I. N. Mishustin, Phys. Rev. **C53** (1996) 1416.

[45] P. K. Sahu, Phys. Rev. **C 62** (2000) 045801.

[46] H. Huber, F. Weber, M. K. Weigel and Ch. Schaab, Int. J. Mod. Phys. **E 7** (1998) 301.

[47] M. Baldo, G. F. Burgio, and H. -J. Schulze, Phys. Rev. **C 58** (1998) 3688 ; *ibid* **C 61** (2000) 055801.

[48] I. Vidaña, A. Polls, A. Ramos, M. Hjorth-Jensen and V. G. J. Stoks, Phys. Rev. **C 61** (2000) 025802;
I. Vidaña, A. Polls, A. Ramos, L. Engvik and M. Hjorth-Jensen, Phys. Rev. **C 62** (2000) 035801.

[49] S. Balberg and A. Gal, Nucl. Phys. **A625** (1997) 435.

[50] S. Balberg, I. Lichtenstadt and G. B. Cook, Astrophys. J. Suppl. **121** (1999) 515.

[51] S. Nishizaki, Y. Yamamoto and T. Takatsuka, Prog. Theor. Phys. **105** (2001), in press.

[52] S. Pal, M. Hanauske, I. Zakout, H. Stöcker and W. Greiner, Phys. Rev. **C 60** (1999) 015802.

[53] M. Hanauske, D. Zschiesche, S. Pal, S. Schramm, H. Stöcker and W. Greiner, Astrophys. J. **537** (2000) 958.

[54] W. Keil and H.-Th. Janka, Astron. Astrophys. **296** (1995) 145 .

[55] J. A. Pons, et al, Astrophys. J. **513** (1999) 780.

[56] M. Prakash, M. Prakash, J. M. Lattimer, and C. J. Pethick, Astrophys. J. **390** (1992) L77.

[57] G. E. Brown, C.- H. Lee and R. Rapp, Nucl. Phys. **A639** (1998) 455c.

[58] T. Muto, Prog. Theor. Phys. **89** (1993) 415.

[59] E. E. Kolomeitsev, D. N. Voskresensky and B. Kämpfer, Nucl. Phys. **A588** (1995) 889.

[60] T. Muto, Proceedings of the VII International Conference on Hypernuclear and Strange Particle Physics, Torino, Italy, October 23-27,2000, to be published in Nucl. Phys. **A**.

[61] H. Yabu, S. Nakamura, F. Myhrer and K. Kubodera, Phys. Lett. **B 315** (1993) 17.

[62] C. H. Lee, H. Jung, D. -P. Min and M. Rho, Phys. Lett. **B 326** (1994) 14.

[63] H. Yabu, F. Myhrer and K. Kubodera, Phys. Rev. **D 50** (1994) 3549.

[64] V. Thorsson and A. Wirzba, Nucl. Phys. **A 589** (1995) 633.

[65] T. Muto, unpublished.

[66] J. C. Ramon, N. Kaiser, S. Wetzel and W. Weise, Nucl. Phys. **A 672** (2000) 249.

[67] M. F. M. Lutz and E. E. Kolomeitsev, nucl-th/0004021.

[68] C. -K. Au and G. Baym, Nucl. Phys. **A 236** (1974) 500.

[69] R. Mittet and E. Østgaard, Phys. Rev. **C 37** (1988) 1711.

[70] J. Boguta, Phys. Lett. **B 106** (1981) 255.

[71] J. M. Lattimer, C. J. Pethick, M. Prakash and P. Haensel, Phys. Rev. Lett. **66** (1991) 2701.

[72] D. J. Millener, C. B. Dover and A. Gal, Phys. Rev. **C 58** (1998) 22700.

[73] T. Fukuda et al., Phys. Rev. **C58** (1998) 1306.

[74] P. Khaustov et al., Phys. Rev. **C 61** (2000) 054603.

[75] J. Dabrowski, Phys. Rev. **C 60** (1999) 025205.

[76] S. Bart et al., Phys. Rev. Lett. **83** (1999) 5238.

[77] J. Mares, E. Friedman, A. Gal and B. K. Jennings, Nucl. Phys. **A 594** (1995) 311.

- [78] M. Kohno, Y. Fujiwara, T. Fujita, C. Nakamoto and Y. Suzuki, Nucl. Phys. **A 674** (2000) 229.
- [79] A. B. Migdal, Rev. Mod. Phys. **50** (1978) 107.
- A. B. Migdal, E. E. Saperstein, M. A. Troitsky and D. N. Voskresensky, Phys. Rep. **192** (1990) 179.
- [80] G. Baym and D. K. Campbell, in *Meson and Nuclei*, ed. M. Rho and D. H. Wilkinson, (North Holland, Amsterdam, 1979), Vol. III, p. 1031.
- [81] T. Ericson and W. Weise, “Pions and Nuclei”, (Clarendon Press, Oxford, 1988).
- [82] T. Kunihiro, T. Muto, T. Takatsuka, R. Tamagaki and T. Tatsumi, Prog. Theor. Phys. Suppl. **112** (1993).
- [83] J. H. Taylor and J. M. Weisberg, Astrophys. J. **345** (1989) 434.
- [84] S. E. Thorsett and D. Chakrabarty, Astrophys. J. **512** (1999) 288.
- [85] M. C. Miller, F. K. Lamb and D. Psaltis, Astrophys. J. **508** (1998) 791.

FIGURES

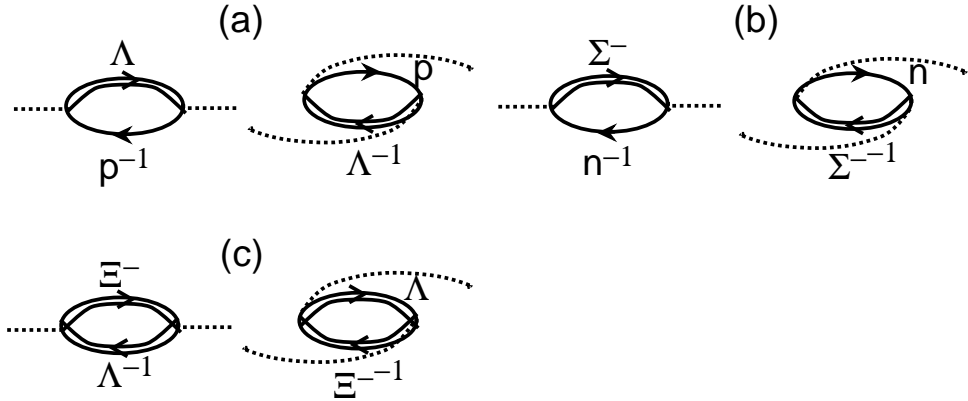


FIG. 1. Pole contributions to the K^- self energy from the p -wave kaon-baryon interactions: (a) Λ -particle-proton-hole and proton-particle- Λ -hole states, (b) Σ^- -particle-neutron-hole and neutron-particle- Σ^- -hole states, and (c) Ξ^- -particle- Λ -hole and Λ -particle- Ξ^- -hole states.

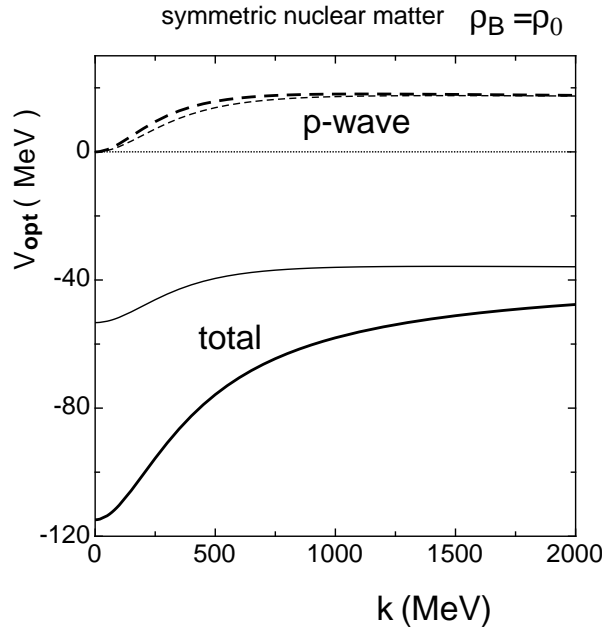


FIG. 2. The K^- optical potential at $\rho_B = \rho_0$ in symmetric nuclear matter.

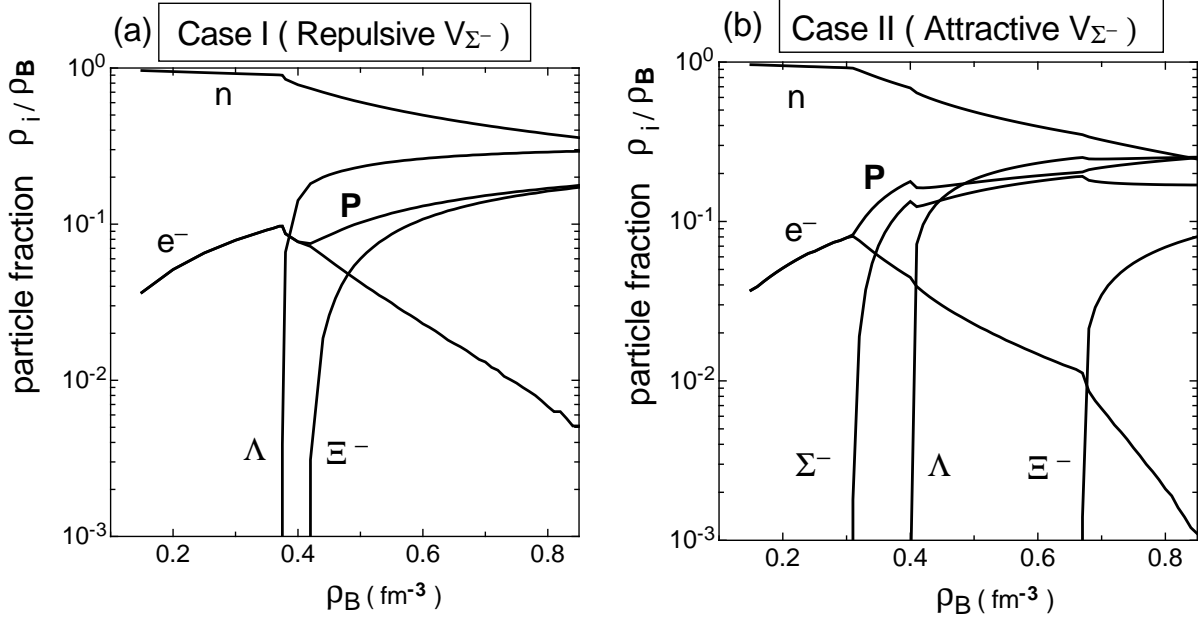


FIG. 3. Particle fractions ρ_i/ρ_B as functions of the baryon number density ρ_B for (a) Case I (the repulsive V_{Σ^-}) and (b) Case II (the attractive V_{Σ^-}).

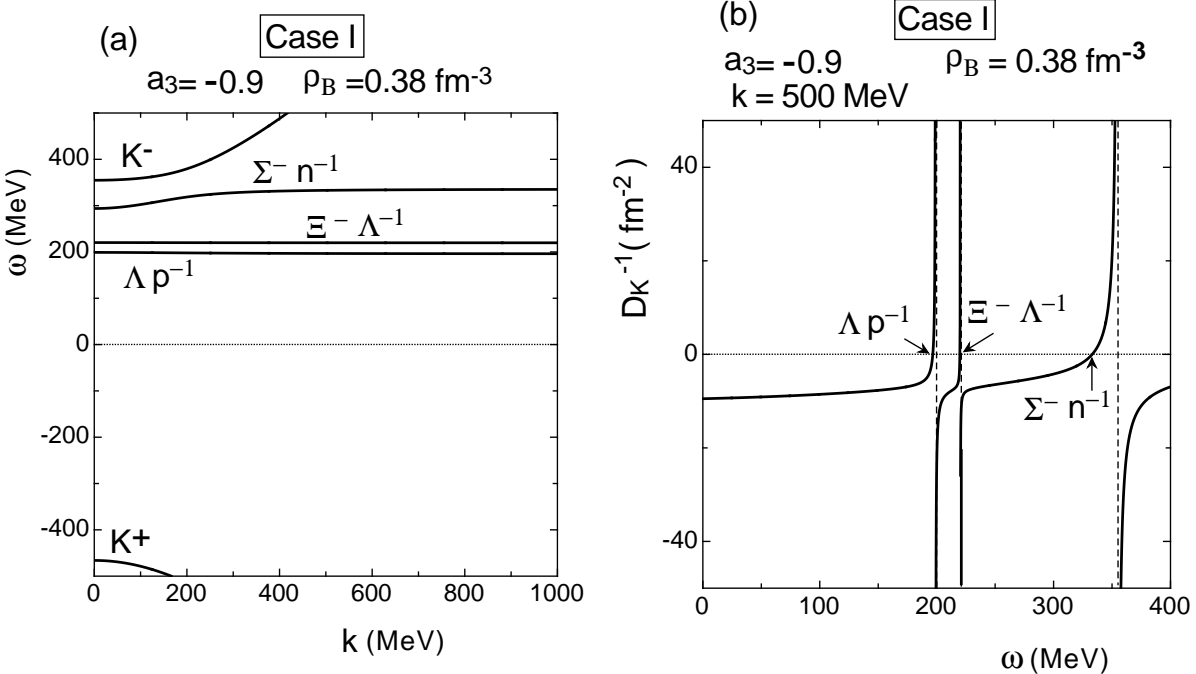


FIG. 4. (a) The excitation energies for kaonic modes as functions of the kaon momentum $|k|$ for $a_3 = -0.9$ ($\Sigma_{Kn} = 305$ MeV) and the baryon number density $\rho_B = 0.38 \text{ fm}^{-3}$. (b) The value of the inverse kaon propagator D_K^{-1} as a function of the excitation energy ω at $|k| = 500$ MeV for the same a_3 and density as Fig. 4 (a).

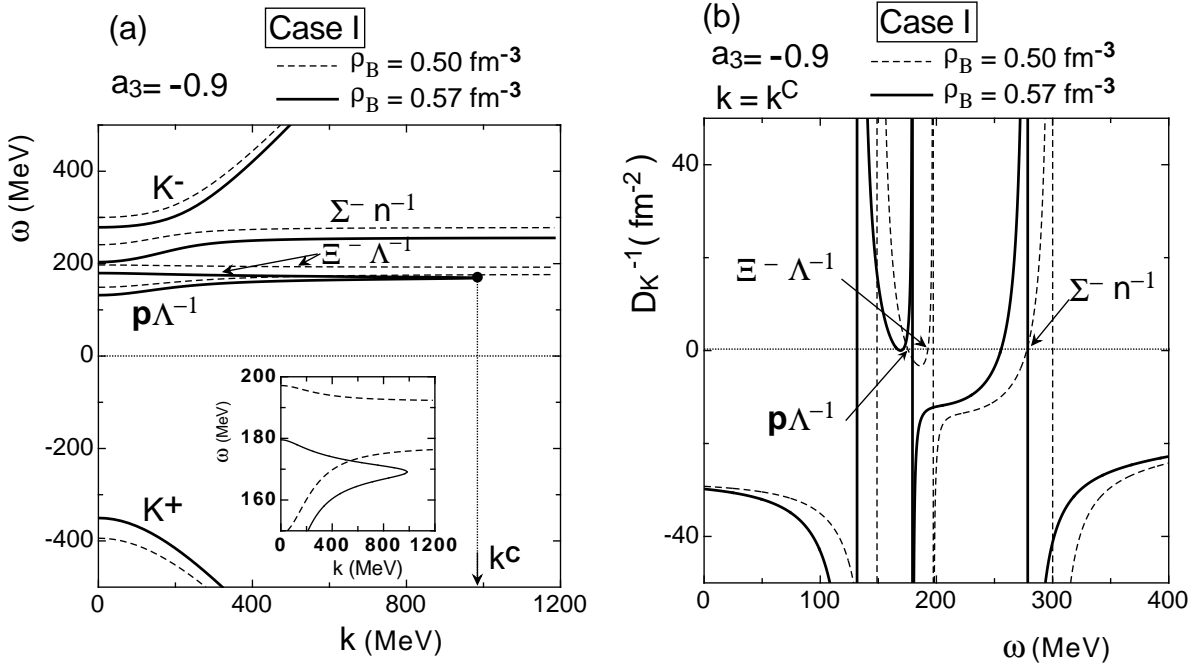


FIG. 5. (a) The excitation energies for kaonic modes as functions of $|k|$ for $a_3 = -0.9$ and $\rho_B = 0.50 \text{ fm}^{-3}$ (dashed line) and $\rho_B = 0.57 \text{ fm}^{-3}$ (solid line). (b) The inverse kaon propagator $D_K^{-1}(\omega, \mathbf{k}; \rho_B)$ as a function of ω at $|\mathbf{k}| = k^C$ ($= 984 \text{ MeV}$) for the same a_3 and ρ_B as in Fig. 5 (a).

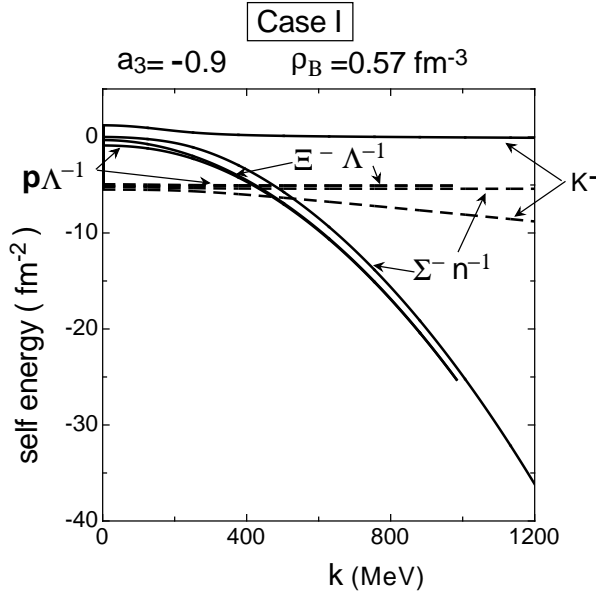


FIG. 6. Contributions to the kaon self energy $\Pi_K(\omega, \mathbf{k}; \rho)$ from the p -wave (solid lines) and s -wave (dashed lines) kaon-baryon interactions for the kaonic modes as a function of $|k|$ for $a_3 = -0.9$ and $\rho_B = 0.57 \text{ fm}^{-3}$ in Case I.

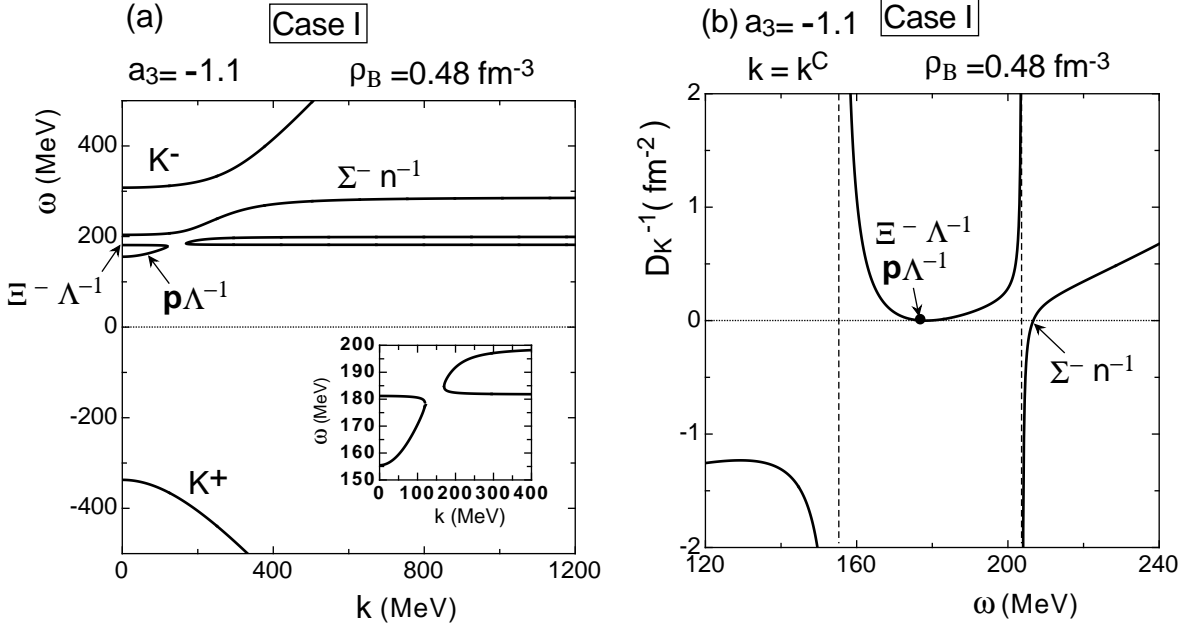


FIG. 7. (a) The excitation energies of kaonic modes as functions of $|k|$ for $a_3 = -1.1$ ($\Sigma_{Kn}=403$ MeV) and $\rho_B=0.48 \text{ fm}^{-3}$ just beyond the onset of condensation in Case I. (b) The value of the kaon inverse propagator $D_K^{-1}(\omega, \mathbf{k}; \rho_B)$ as a function of ω at $|\mathbf{k}| = k^C=118$ MeV. The values of a_3 and ρ_B are the same as those in Fig. 7 (a).

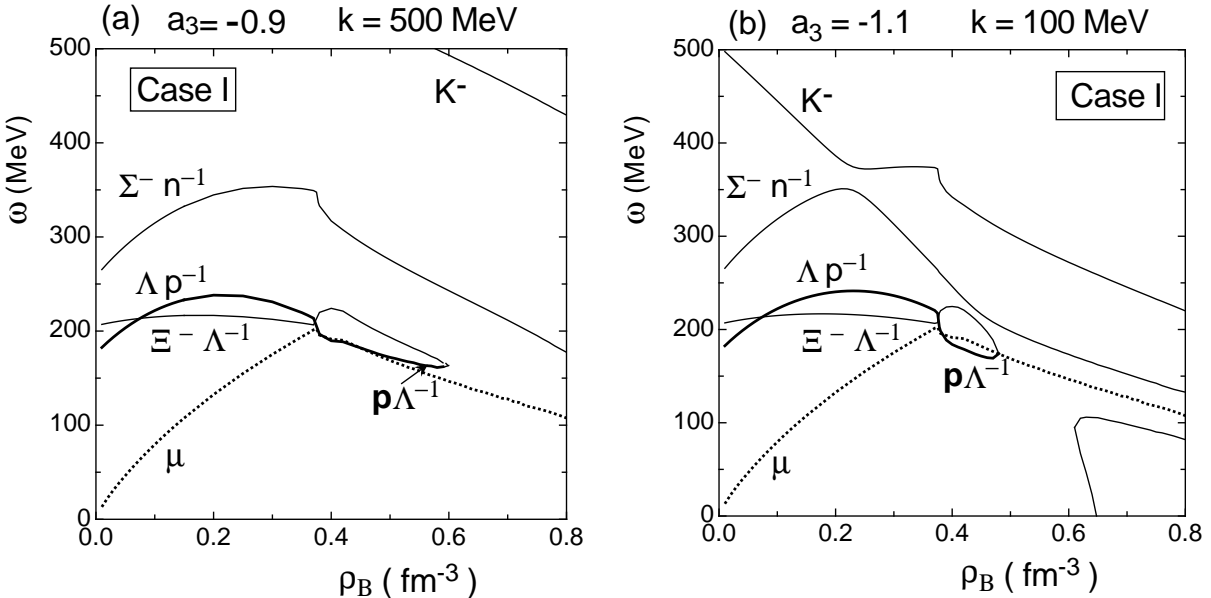


FIG. 8. (a) The dependence of the excitation energies of kaonic modes on the baryon number density for $a_3 = -0.9$ ($\Sigma_{Kn}=305$ MeV) and $|\mathbf{k}|=500$ MeV in Case I. The charge chemical potential μ is also shown as a function of ρ_B by a dotted line. (b) The same as Fig. 8 (a), but for $a_3 = -1.1$ ($\Sigma_{Kn}=403$ MeV) and $|\mathbf{k}|=100$ MeV. The charge chemical potential μ (the dotted line) is identical to that in Fig. 8 (a).

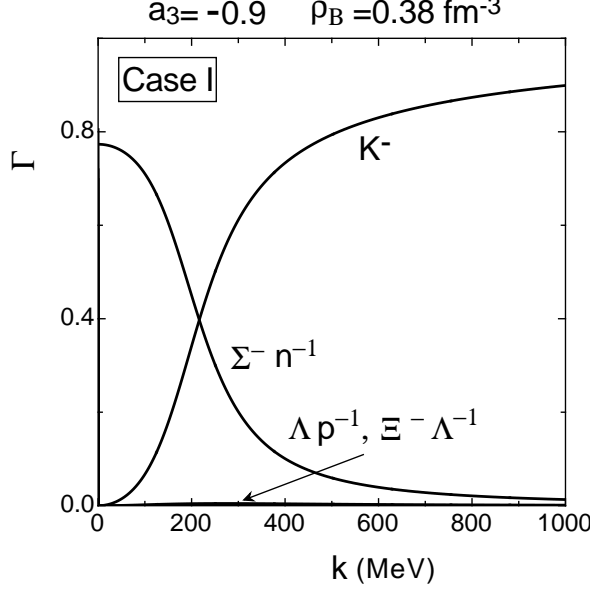


FIG. 9. Occupation factors $\Gamma(i) \equiv 2\omega(\partial D_K^{-1}/\partial\omega)^{-1}|_{\omega=\omega_i}$ for the kaonic modes ($i = K^-, \Lambda p^{-1}, \Sigma^- n^{-1}, \Xi^- \Lambda^{-1}$) as functions of $|\mathbf{k}|$ for $a_3 = -0.9$ and $\rho_B = 0.38 \text{ fm}^{-3}$ in Case I.

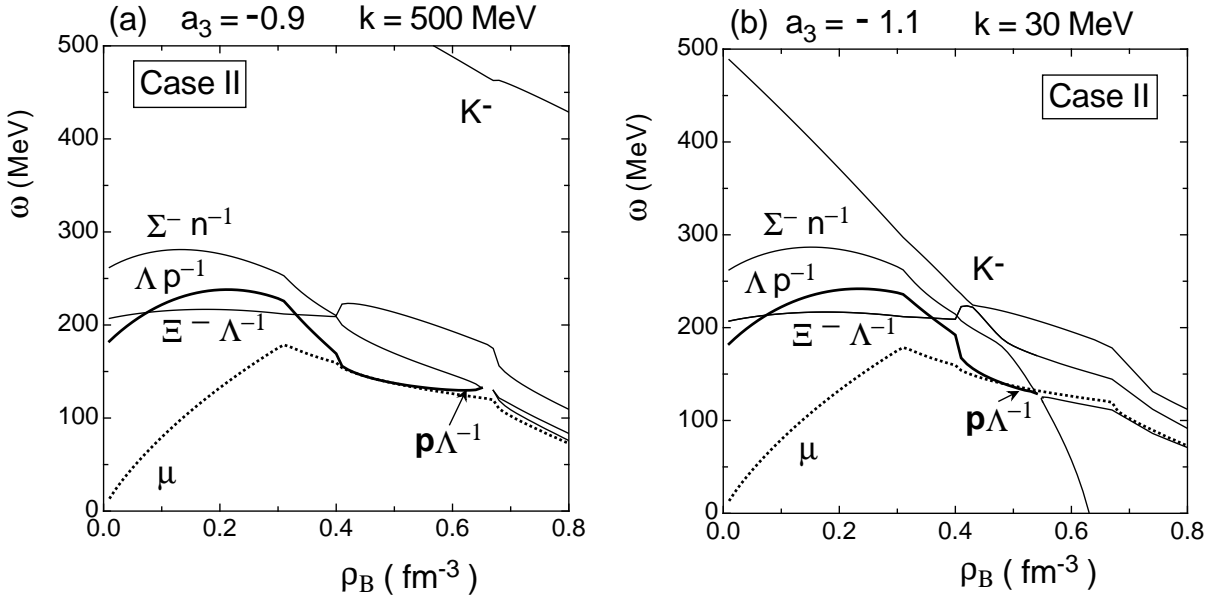


FIG. 10. (a) The dependence of the excitation energies of kaonic modes on the baryon number density for $a_3 = -0.9$ ($\Sigma_{Kn} = 305 \text{ MeV}$) and $|\mathbf{k}| = 500 \text{ MeV}$ in Case II. The charge chemical potential μ is also shown as a function of ρ_B by a dotted line. (b) The same as Fig. 10 (a), but for $a_3 = -1.1$ ($\Sigma_{Kn} = 403 \text{ MeV}$) and $|\mathbf{k}| = 30 \text{ MeV}$. The charge chemical potential μ (the dotted line) is identical to that in Fig. 10 (a).

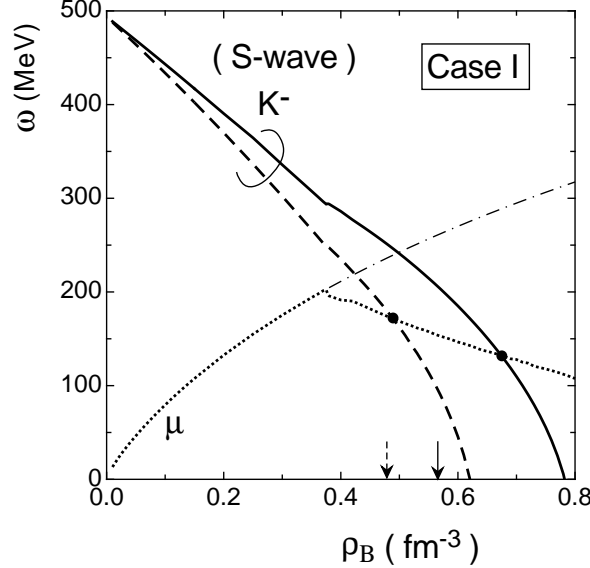


FIG. 11. The dependence of the minimum excitation energy of the s -wave K^- on the baryon number density for $|\mathbf{k}| = 0$ in Case I. The solid line is for $a_3 = -0.9$ and the dashed line is for $a_3 = -1.1$. The charge chemical potential μ (the dotted line) is identical to that in Fig. 8. For reference, the charge chemical potential in neutron-star matter consisting of only the nucleons n , p and e^- is shown by the dash-dotted line.

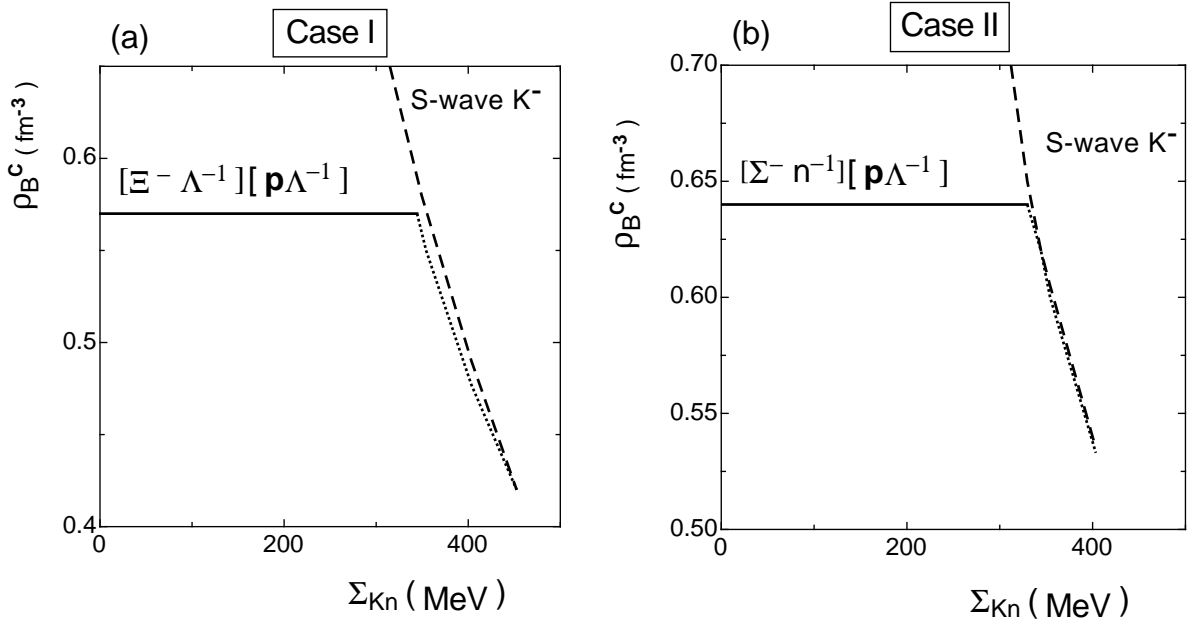


FIG. 12. (a) The critical density of the p -wave kaon condensation (the solid and dotted lines) as a function of the kaon-neutron sigma term Σ_{Kn} in Case I. For comparison, the critical density for the s -wave K^- condensation is shown by the dashed line. (b) The same as (a), but for Case II. See the text for the details.

TABLES

TABLE I. Parameters in the potential energy density. (^aMeV·fm³, ^bMeV·fm³)

parameter		parameter		parameter	
γ	5/3	$a_{\Lambda N}^a$	-387.0	a_{YY}^a	-552.6
δ	5/3	$c_{\Lambda N}^b$	738.8	c_{YY}^b	1055.4
a_{NN}^a	-859.5	$a_{\Xi N}^a$	-228.6	$b_{\Xi\Xi}^a$	0
b_{NN}^a	212.8	$b_{\Xi N}^a$	0	$b_{\Sigma\Xi}^a$	0
c_{NN}^b	1300.8	$c_{\Xi N}^b$	436.5	$b_{\Sigma\Sigma}^a$	428.4

TABLE II. Parameters for the $\Sigma^- N$ part in the potential energy density. (^aMeV·fm³, ^bMeV·fm³)

	Case I	Case II
$a_{\Sigma N}^a$	-70.9	-387.0
$b_{\Sigma N}^a$	251.3	214.2
$c_{\Sigma N}^b$	738.8	738.8